

1           **Continuity of global MODIS terrestrial primary  
2           productivity estimates in the VIIRS era using  
3           model-data fusion**

4           **K. Arthur Endsley<sup>1</sup>, Maosheng Zhao<sup>2</sup>, John S. Kimball<sup>1</sup>, Sadashiva Devadiga<sup>3</sup>**

5           <sup>1</sup>Numerical Terradyamic Simulation Group (NTSG), W.A. Franke College of Forestry and Conservation,  
6           University of Montana, Missoula, MT, U.S.A.

7           <sup>2</sup>Science Systems and Applications, Inc.  
8           <sup>3</sup>NASA Goddard Space Flight Center, Greenbelt, MD, U.S.A.

9           **Key Points:**

- 10          • Over two decades of global productivity estimates from MODIS cannot be con-  
11          tinued without use of VIIRS data.
- 12          • We performed a comprehensive calibration and validation, and sensitivity and un-  
13          certainty analyses of MODIS MOD17 and new VIIRS VNP17.
- 14          • Both MOD17 and new VNP17 depict upward productivity trends and mean and  
15          interannual variability consistent with independent data.

16 **Abstract**

17 The NASA Terra and Aqua satellites have been successfully operating for over two decades,  
 18 exceeding their original 5-year design life. However, the era of NASA's Earth Observing System (EOS)  
 19 may be coming to a close as early as 2023. Similarities between the  
 20 Moderate Resolution Imaging Spectroradiometer (MODIS), aboard Aqua and Terra, and  
 21 the Visible Infrared Imaging Radiometer Suite (VIIRS) sensors aboard the Suomi NPP,  
 22 NOAA-20 and NOAA-21 satellites enable potential continuity of long-term earth observational  
 23 records in the VIIRS era. We conducted a comprehensive calibration and validation  
 24 of the MODIS MOD17 product, which provided the first global, continuous, weekly  
 25 estimates of ecosystem gross primary productivity (GPP) and annual estimates of net  
 26 primary productivity (NPP). Using Bayesian model-data fusion, we combined an 18-year  
 27 record of tower fluxes with prior data on plant traits and hundreds of field measurements  
 28 of NPP to benchmark MOD17 and to develop the first terrestrial productivity estimates  
 29 from VIIRS. The updated mean global GPP (NPP) flux from MOD17 and the new VNP17  
 30 for 2012-2018 is  $127 \pm 2.8 \text{ Pg C year}^{-1}$  ( $58 \pm 1.1 \text{ Pg C year}^{-1}$ ), which compares well with  
 31 independent top-down and bottom-up estimates. Both MOD17 and VNP17 depict up-  
 32 ward productivity trends over recent decades, with 2000-2018 MOD17 GPP (NPP) rising  
 33 by  $0.47$  ( $0.25$ )  $\text{Pg C year}^{-2}$  but slowing to  $0.35$ - $0.44$  ( $0.11$ - $0.13$ )  $\text{Pg C year}^{-2}$  over 2012-  
 34 2021, with a greater reduction in the NPP growth rate. The new VIIRS VNP17 prod-  
 35 uct has the potential to extend these continuous estimates of global, terrestrial primary  
 36 productivity beyond 2030.

37 **Plain Language Summary**

38 The NASA Terra and Aqua satellites have been successfully operating for over two  
 39 decades, far longer than their original 5-year design life. However, one or both satellites  
 40 may run out of fuel as early as 2023. These satellites carry the Moderate Resolution Imag-  
 41 ing Spectroradiometer (MODIS) sensors, which are very similar to the Visible Infrared  
 42 Imaging Radiometer Suite (VIIRS) sensors aboard newer satellites. The long record of  
 43 MODIS data collected so far may therefore be extended by the VIIRS sensors, partic-  
 44 ularly the global estimates of the amount of carbon in the atmosphere taken up and stored  
 45 by plants. We used multiple independent datasets to figure out if and how the MODIS  
 46 MOD17 computer model should be changed to improve its accuracy and to use data from  
 47 VIIRS. The new VIIRS VNP17 data could extend our record of plant-atmosphere car-  
 48 bon exchange beyond the year 2030.

49 **1 Introduction**

50 The Moderate Resolution Imaging Spectroradiometer (MODIS), carried by the Terra  
 51 and Aqua satellites, is a key component of NASA's Earth Observing System (EOS) (Justice  
 52 et al., 2002), which has contributed observations of Earth's land, atmosphere, and oceans  
 53 for over two decades. Although Terra and Aqua have far exceeded their original 5-year  
 54 design life, the end of the EOS era is near, as one or both of the satellites may run out  
 55 of fuel as early as 2023. Because of the dozens of products derived from the 36 MODIS  
 56 spectral bands, and because of the similarity of the Visible Infrared Imaging Radiome-  
 57 ter Suite (VIIRS) sensor aboard the Suomi NPP and NOAA-20 satellites, there has long  
 58 been interest in using VIIRS to provide continuity of land surface observations (Murphy  
 59 et al., 2001; Xiong et al., 2020). MODIS-like observations will continue to be important  
 60 for global studies of terrestrial productivity, including ecosystem monitoring (Y. Zhang,  
 61 Song, et al., 2017; M. O. Jones et al., 2020) and agricultural studies (Skakun et al., 2018).

62 Of particular interest are the on-going applications of MODIS to studies of the ter-  
 63 restrial carbon cycle, beginning with the first global, continuous, weekly estimates of ecosys-  
 64 tem gross primary productivity (GPP) and annual estimates of net primary productiv-  
 65 ity (NPP): the Terra MODIS MOD17 product (Running et al., 2004; Zhao et al., 2005).

The MOD17 product, now exceeding 22 years of record, has been instrumental in diagnosing increasing water limitations on carbon uptake (Zhao & Running, 2010), highlighting the role of humans in wildfire ignition (Balch et al., 2017), and constraining human appropriations of biomass (Erb et al., 2018), among other diverse applications. It is no coincidence that MOD17 was developed at the same time that direct, ecosystem-level measurements of canopy gas exchange from eddy covariance (EC) flux towers first became widely available (Baldocchi et al., 2001). The simple light-use efficiency (LUE) approach allows for up-scaling the ecosystem-level estimate of GPP from towers using satellite observations of canopy vigor and gridded surface meteorological data (Ryu et al., 2019).

Here, we confront the MOD17 GPP and NPP models with data in a comprehensive calibration and validation study. We also present the first calibration and assessment of the MOD17 algorithm for use with the VIIRS sensor, enabling continuity of multi-decadal GPP and NPP estimates. The independent observational data used in this study include eddy covariance (EC) tower CO<sub>2</sub> fluxes, field surveys of productivity and biomass change, and a global database of species-level plant traits (Kattge et al., 2020). Previous MOD17 calibration efforts prescribed a set of general biophysical response characteristics for major land cover types, defined in the model's Biome Properties Look-up Table (BPLUT), and derived using a limited set of EC tower site observations as well as literature review, expert elicitation, and a smaller set of NPP estimates (Zhao et al., 2005). Here, we conducted a more extensive model calibration and formal analysis of model sensitivity and uncertainty in parameterization, which has been performed for similar diagnostic models (e.g., L. A. Jones et al., 2017; K. Zhang et al., 2019), but not yet for MOD17.

## 2 Data and Methods

Although there is a file-naming convention where “MOD” indicates a product granule based on Terra MODIS data (only, as opposed to Aqua MODIS), we use “MOD17” throughout this paper to refer to the combined GPP/NPP algorithm, which is currently operational using MODIS observations from both EOS Terra and Aqua satellites.

### 2.1 The MOD17 Algorithm

As MOD17 has been discussed thoroughly in the literature, we give only a brief overview of the model here. A complete description is available in the MOD17 Collection 6.1 User’s Guide (Running & Zhao, 2021). MOD17 consists of three potentially independent sub-models: 8-day GPP, 8-day net photosynthesis (PSN<sub>net</sub>), and annual NPP. 8-day composite products are given the designation MOD17A2H, for Terra MODIS, or MYD17A2H, for Aqua MODIS. Annual products, including annual GPP (the sum of one year’s 8-day GPP composites), are carried by MOD17A3H (or MYD17A3H). GPP is calculated using a classic light-use efficiency (LUE) approach (Running et al., 2004; Yuan et al., 2014; Madani et al., 2017), where the carbon (C) uptake by plants is assumed to be proportional to canopy absorbed photosynthetically active radiation (APAR) under prevailing daytime environmental conditions for diel or longer time scales. Low temperatures or high vapor pressure deficit (VPD) reduce the efficiency of photosynthetic C uptake, thus, MOD17 GPP is described as a product of APAR, the light-use efficiency under optimal conditions ( $\varepsilon_{\max}$ ), and environmental scalars:

$$\text{GPP} = \text{APAR} \times \varepsilon_{\max} \times f(T_{\min}) \times f(\text{VPD}) \quad (1)$$

Where  $f(T_{\min})$  and  $f(\text{VPD})$  are numbers on [0, 1] representing the decline in  $\varepsilon_{\max}$  due to low daily minimum temperatures and high VPD, respectively. These environmental scalars are represented as linear ramp functions, where limiting conditions are interpolated between zero (completely limiting, i.e., photosynthesis cannot occur) and one (non-limiting). The key parameters in modeling GPP, in addition to  $\varepsilon_{\max}$ , are the  $T_{\min}$

115 and VPD values that indicate the width of the ramp function and, consequently, the slope  
 116 that determines how much  $\varepsilon_{\max}$  is reduced for a unit decrease in  $T_{\min}$  or unit increase  
 117 in VPD.

118 Daily (or 8-day) net photosynthesis is calculated as GPP less maintenance respi-  
 119 ration ( $R_M$ ) from leaves and fine roots. Leaf  $R_M$  is based on a Q10 function (Tjoelker  
 120 et al., 2001) and the current leaf C mass, which is estimated instantaneously as leaf area  
 121 index (LAI) divided by specific leaf area (SLA). Fine root  $R_M$  is also based on a Q10  
 122 function and the fine root C mass is based on an allometric relationship with the leaf C  
 123 mass. The same Q10  $\equiv 2$  is used for fine roots and livewood whereas leaves use a temperature-  
 124 acclimated equation (ibid.). Notably, as MOD17 does not track biomass allocation, live-  
 125 wood respiration and growth respiration,  $R_G$ , are not included in PSN<sub>net</sub>. Annual NPP  
 126 does account for  $R_G$  and livewood  $R_M$ , estimating livewood C mass through an allomet-  
 127 ric relationship with annual maximum leaf C mass. Based on empirical studies,  $R_G$  is  
 128 estimated to consume 25% of annual NPP; thus, annual NPP is calculated as:

$$129 \quad \text{NPP} = \text{GPP} - R_M - R_G = \frac{1}{1.25}(\text{GPP} - R_M) \quad (2)$$

130 The complete list of parameters is included in Table 1. Each of the parameters is  
 131 defined separately for 11 distinct plant functional types (PFTs), based on the MODIS  
 132 MCD12Q1 Type 2 International Geosphere-Biosphere Programme (IGBP) land-cover  
 133 classification (Friedl & Sulla-Menashe, 2019; Sulla-Menashe et al., 2019).

134 MOD17 Collection 6.1 (C61) depends on surface meteorological data including mean  
 135 and minimum daily air temperature, photosynthetically active radiation (PAR), atmo-  
 136 spheric pressure, and the water vapor mixing ratio. These inputs are derived from the  
 137 NASA Global Modeling and Assimilation Office (GMAO) Goddard Earth Observing Sys-  
 138 tem 5 (GEOS-5), Forward Processing for Instrument Teams (GEOS FP-IT). It also de-  
 139 pends on driver data from MOD15A2H (Myneni et al., 2015), a record of LAI and the  
 140 fraction of the canopy absorbing PAR (fPAR). Taken together, these data determine the  
 141 surface cover available to harvest light for C (CO<sub>2</sub>) uptake and the environmental con-  
 142 straints on that process.

143 In this re-processing, there are some significant departures from earlier versions of  
 144 MOD17. First, C61 and all previous versions of MOD17 used an estimate of short-wave  
 145 radiation (GMAO “SWGNT”) that is likely too low to be used in calculating PAR. Es-  
 146 timation of PAR is based on irradiance measurements indicating that approximately 45%  
 147 of the daily (short-wave) solar irradiance is within the PAR waveband, 400-700 nm (Meek  
 148 et al., 1984). However, MOD17 has historically used 45% of *net* short-wave radiation for  
 149 calculating PAR, which might be an underestimate, as SWGNT accounts for surface albedo.  
 150 Based on GMAO data over 2000-2017, the incoming daily short-wave irradiance (GMAO  
 151 “SWGDN”) is always greater than or equal to SWGNT. Previous MOD17 calibration  
 152 (Zhao et al., 2005, 2006) has likely compensated for this underestimation of PAR.

153 Here, we re-calibrate MOD17 using GMAO SWGDN instead of SWGNT. In ad-  
 154 dition, whereas C61 and prior versions have fixed fine-root and livewood Q10 values at  
 155 2, we make these free parameters during model calibration, based on prior evidence that  
 156 suggest this fixed value may be suboptimal (see “Model-Data Fusion”). Prior to calibra-  
 157 tion, we conducted a global sensitivity analysis of MOD17’s free parameters, based on  
 158 the Sobol’ variance-based decomposition method (Sobol’, 2001). This was performed in  
 159 Python using SALib (Herman & Usher, 2017; Iwanaga et al., 2022), and obtains the pro-  
 160 portion of the total variance in GPP or NPP that is contributed directly by a given pa-  
 161 rameter or by an interaction between that parameter and any combination of other pa-  
 162 rameters.

Table 1: Free parameters in MOD17, with units and a short description.

Parameter	Units	Description
$\varepsilon_{\max}$	$\text{kg C MJ}^{-1}$	LUE under optimal conditions
$T_{\min,\leftarrow}$	deg Celsius	Minimum temperature below which $\varepsilon = 0$
$T_{\min,\rightarrow}$	deg Celsius	Minimum temperature above which $\varepsilon$ not limited by temperature
$\text{VPD}_{\leftarrow}$	Pa	VPD below which $\varepsilon$ is not limited by VPD
$\text{VPD}_{\rightarrow}$	Pa	VPD above which $\varepsilon = 0$
$\text{SLA}$	$(\text{kg C})^{-1}$	Projected leaf area per unit mass of leaf C
$\text{froot\_leaf\_ratio}$		Allometric ratio of fine root C to leaf C
$\text{livewood\_leaf\_ratio}$		Allometric ratio of livewood C to leaf C
$\text{leaf\_mr\_base}$	$\text{kg C } (\text{kg C})^{-1} \text{ day}^{-1}$	Maintenance respiration base rate, per unit leaf C, at 20 deg C
$\text{froot\_mr\_base}$	$\text{kg C } (\text{kg C})^{-1} \text{ day}^{-1}$	Maintenance respiration base rate, per unit fine root C, at 20 deg C
$\text{livewood\_mr\_base}$	$\text{kg C } (\text{kg C})^{-1} \text{ day}^{-1}$	Maintenance respiration base rate, per unit livewood C, at 20 deg C
$Q10\_froot$		Exponent shape parameter relating fine root $R_M$ to temperature
$Q10\_livewood$		Exponent shape parameter relating livewood $R_M$ to temperature

163        **2.2 Model Calibration Data**

164        For GPP model calibration, we used a globally representative network of 352 eddy  
 165        covariance (EC) flux towers from the FLUXNET/La Thuile synthesis collection (Baldocchi,  
 166        2008). Based on a recent analysis of EC tower footprints (Chu et al., 2021), we chose a  
 167        conservative tower footprint of 1.5 km, or a 3-by-3 grid of 500-m pixels centered on the  
 168        tower. This area is used to integrate fPAR and LAI observations at 500-m scale and smooth  
 169        the resulting GPP predictions through spatial averaging. Tower daily gap-filled GPP data  
 170        were smoothed using a 2-day moving window filter with zero phase offset and observa-  
 171        tions were discarded when PAR was below  $0.1 \text{ MJ m}^{-2}$  per day. fPAR and LAI data were  
 172        filtered to remove spurious spikes; low-quality fPAR and LAI data, based on the qual-  
 173        ity check (QC) band, were filled in from an fPAR or LAI climatology. Then, 8-day fPAR  
 174        and LAI were interpolated to daily time steps using forward and backward filling. In ad-  
 175        dition to MODIS MOD15A2H fPAR and LAI, daily surface meteorological data were com-  
 176        piled for tower sites for the years 2000 through 2017 from the Modern-Era Retrospec-  
 177        tive Re-analysis (MERRA-2, Gelaro et al., 2017).

178        MOD17 is calibrated separately for each PFT. Each FLUXNET site is assigned a  
 179        dominant PFT, the class that makes up the majority of 500-m pixels within the 1.5-km  
 180        tower footprint. Tower sites used for model calibration were screened to ensure PFT con-  
 181        sistency between the local tower footprints and overlying MOD17 windows. Calibration  
 182        for a given PFT uses just those FLUXNET sites where that PFT is dominant (Table 2).  
 183        Because no FLUXNET site is located within a majority-DNF canopy, we assigned to this  
 184        PFT two majority-ENF sites that have DNF pixels within a 3-km radius. CSH is also  
 185        poorly represented among FLUXNET sites, dominant at only 2 sites. We assigned 3 other  
 186        sites that have CSH pixels within the 1.5-km footprint, but which are dominant elsewhere.

Table 2: The plant functional type (PFT) classification used in MOD17, which is based on the MODIS MCD12Q1 Type 2 classification. The number of FLUXNET sites with each PFT as the dominant ground cover (i.e., majority of 500-m pixels within a 1.5-km footprint) is also included.

Plant Functional Type (PFT)	Abbreviation	Number of FLUXNET sites
Evergreen needleleaf forest	ENF	30
Evergreen broadleaf forest	EBF	22
Deciduous needleleaf forest	DNF	2
Deciduous broadleaf forest	DBF	32
Mixed forest	MF	33
Closed shrublands	CSH	5
Open shrublands	OSH	15
Woody savannas	WSV	47
Savannas	SAV	35
Grasslands	GRS	77
Croplands	CRO	54

187        Annual NPP parameters have never before been directly calibrated against obser-  
 188        vations, with model misfit quantified by the difference between predictions and field es-  
 189        timates of NPP. Here, we use a multi-decadal inventory of global NPP estimates collected  
 190        by the Oak Ridge National Laboratory (ORNL) Distributed Active Archive Center (DAAC).  
 191        This “Multi-Biome” collection and other field datasets (Table 3) describe above-ground,  
 192        below-ground, and/or total NPP at over 1,600 field sites, providing a basis for global cal-  
 193        ibration of terrestrial carbon models. There are some challenges, however.

194        Few of the datasets in this collection provide details on the land-use or manage-  
 195        ment history and fewer still provide specific years or year ranges for the NPP estimates;

Table 3: Calibration and validation data used in this study, with citations. The majority of datasets come from the Oak Ridge National Laboratory (ORNL) Distributed Active Archive Center (DAAC). The last two entries refer to separate published papers.

Dataset	Citation
Summary Data from Intensive Studies at 125 Sites, 1936-2006	(Olson et al., 2017)
Global Osnabruck Data, 1937-1981, R1	(Esser, 2013)
Grassland, Boreal Forest, and Tropical Forest Sites, 1939-1996, R1	(Scurlock & Olson, 2012)
PIK Data for Northern Eurasia, 1940-1988 (Based on Bazilevich), R1	(Dennisenko et al., 2012)
TEM Calibration Data, 1992, R1	(Kicklighter, 2012)
Global IBP Woodlands Data, 1955-1975, R1	(DeAngelis et al., 2012)
Global Primary Production Data Initiative Products, R2	(Olson et al., 2013)
Boreal Forest Consistent Worldwide Site Estimates, 1965-1995, R1	(Gower et al., 2012)
NPP Estimates from Biomass Dynamics for 31 Sites, 1948-1994, R1	(Scurlock et al., 2003)
VAST Calibration Data, 1965-1998, R1	(Barrett, 2012)
“Biomass production...in temperate and boreal ecosystems”	(Campioli et al., 2015)
“Depth distribution of belowground net primary production...”	(Luo et al., 2021)

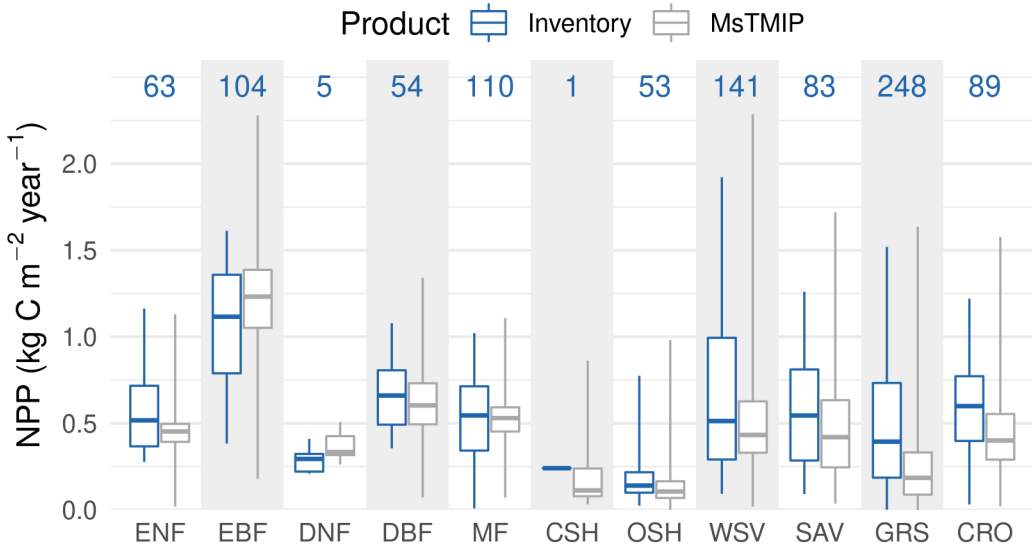


Figure 1: Boxplots of mean annual NPP, by Plant Functional Type (PFT), for the Cal-Val (“Inventory”) data and the MsTMIP ensemble mean, based on a majority resampling of land-cover data to MsTMIP’s half-degree grid. Numbers at top indicate the total number of site-years for the Inventory data. Whiskers show the minimum and maximum of each dataset. Sites with reported mean annual NPP greater than  $2,385 \text{ g C m}^{-2} \text{ year}^{-1}$  were discarded.

the estimates span a range of years from 1936 to 2006. Sites in the inventory were classified into PFT groups based, first, on the reported biome or vegetation type; if no such information was provided, the site coordinates were used to map the PFT class from the MCD12Q1 Type 2 global mosaic for year 2015. A small number of sites were excluded because they did report intensive management histories (fertilizer, irrigation, mowing, or burning). NPP estimates from Gower et al. (2012) and Olson et al. (2013) were grouped by site (unique name or coordinates) and averaged. Because CSH describes such a small proportion of the global land domain (Madani et al., 2017), additional, randomly chosen CSH sites from the NPP validation datasets were added to the calibration dataset. In addition, data compiled by Campioli et al. (2015) and Luo et al. (2021) were added to the ORNL calibration dataset, after removing sites that were duplicated from the ORNL data, resulting in a total of 1,646 annual NPP measurements for calibration and validation (“Cal-Val”).

As we cannot exclude the possibility that some sites are intensively managed to boost productivity (e.g., by fertilization or irrigation), we removed NPP samples that fell outside the PFT-group range of global mean (1980-2000) annual NPP, which was derived from a fusion of annual FLUXCOM NEE (Jung et al., 2020) and heterotrophic respiration ( $R_H$ ) data from X. Tang et al. (2020). After also accounting for sites that fall outside of the MODIS global land domain (i.e., have no fPAR or LAI data), this resulted in a final total of 951 valid NPP measurements. The NPP Cal-Val data show expected differences by PFT and the median NPP agrees well with previously reported biome-level averages (e.g., Kicklighter et al., 1999; Zaks et al., 2007), and also with the Multi-Scale Synthesis and Terrestrial Model Intercomparison Project (MsTMIP, Huntzinger et al., 2013) “BG1” simulation (time-varying climate, land-cover,  $\text{CO}_2$ , and nitrogen deposition) ensemble mean (Figure 1). Reported values in DNF canopy ( $209\text{--}410 \text{ g C m}^{-2}$

221 year<sup>-1</sup>) are low but consistent with reports from field measurements in forest stands (Kushida  
 222 et al., 2007; Ji et al., 2020).

223 Corresponding NPP model meteorological drivers for 1980-2000 were obtained from  
 224 the MERRA-2 re-analysis (Gelaro et al., 2017), which is derived from the GEOS-5 land  
 225 model. As most sites do not specify the exact year of the NPP measurement, we used  
 226 daily data from a randomly chosen year between 1980-2000 for each site, for the corre-  
 227 sponding calendar day of a 365-day year, so as to capture the real, within-site, intra-annual  
 228 variability in environmental drivers (as opposed to reducing the variance by using a cli-  
 229 matology). As MOD17 does not have any state tracked between time steps, and as mod-  
 230 eled NPP is calculated over the synthetic, 365-day year at each site, there are no issues  
 231 with using different days for consecutive years. Because there are no MODIS data prior  
 232 to 2000, MODIS fPAR and LAI climatologies were calculated for the 2000-2005 period  
 233 for use in calibrating annual NPP.

### 234 2.3 Model-Data Fusion

235 The parameters in the MOD17 BPLUT, itemized in Table 1, were previously de-  
 236 rived from literature review and some empirical studies. Today, there are numerous, di-  
 237 rect ecological observations that can be used to inform model development and calibra-  
 238 tion, including extensive EC flux tower data and measured plant traits. We consulted  
 239 the global TRY database (Kattge et al., 2020) for plant traits relevant to MOD17 pa-  
 240 rameters and developed prior parameter distributions for use in a Bayesian model-data  
 241 fusion. Specifically, using Markov Chain Monte Carlo (MCMC), the observed distribu-  
 242 tions of plant traits were used as priors for estimating the likelihood of MOD17 param-  
 243 eters given the difference between modeled and observed GPP or NPP. Details of how  
 244 plant traits informed priors are available in the Supplement.

245 Likelihood-ratio tests indicated that the SLA prior for each PFT was significantly  
 246 different from the pooled distribution (i.e., based on values from all PFTs). We decided  
 247 to fix SLA at its prior mean (from the TRY database), given the thousands of species  
 248 observations for this parameter, because SLA was revealed to be the most sensitive model  
 249 parameter and we believe the TRY data to be more reliable for fixing this parameter than  
 250 the relatively small number of field NPP estimates.

251 Model calibration was performed using MCMC with the Differential Evolution Metropo-  
 252 lis sampler described by Ter Braak and Vrugt (2008) and Vrugt et al. (2009), as imple-  
 253 mented in the PyMC framework (Salvatier et al., 2016). Between 100,000 and 200,000  
 254 samples were drawn from the posterior for each of three chains, based on a root-mean  
 255 squared error (RMSE) pseudo-likelihood function. Chains were qualitatively assessed for  
 256 convergence and required burn-in; thinning to remove autocorrelation was one in every  
 257 20 (for GPP) or 200 (for NPP) samples. The optimal posterior point estimate, used in  
 258 the updated BPLUT, was chosen as the mean *a posteriori* estimate.

### 259 2.4 Inter-calibration for the VIIRS Sensor

260 Within the 2000-2017 period for which FLUXNET data are available, the SNPP  
 261 VIIRS mission provides data for 5 years (2012-2017). Because the VIIRS record is much  
 262 shorter than the MODIS record, and also because of differences in fPAR and LAI be-  
 263 tween the corresponding VNP15A2H and MOD15A2H products, we opted to calibrate  
 264 MOD17 for VIIRS differently. Instead of using data fusion for calibration against ob-  
 265 served NPP (as with the updated MODIS MOD17 product), we derived bias-correction  
 266 coefficients based on systematic differences in fPAR and LAI between the two sensors  
 267 and apply these to the updated MOD17 BPLUT. The ratio between mean MOD15A2H  
 268 fPAR and mean VNP15A2H fPAR is used as a multiplier to adjust the  $\epsilon_{\max}$  parame-  
 269 ter in the resulting VNP17 BPLUT while the ratio between mean MOD15A2H LAI and

mean VNP15A2H LAI is used as a multiplier to adjust the SLA parameter. Besides  $\varepsilon_{\max}$  and SLA, the updated MOD17 and new VNP17 BPLUT would be the same.

In deriving both coefficients, because GPP is only accumulated for part of the year (but  $R_M$  continues year-round), we calculated mean fPAR and LAI only during the growing season, defined as days when the daily temperature constraint on GPP (defined by  $T_{\min,\leftarrow}$ ) is above zero. The input fPAR and LAI data to this process are the 5-km gap-filled datasets used for global simulation (see “Global Boundary Conditions” section). The fPAR-based  $\varepsilon_{\max}$  coefficients range from 0.965 (ENF) to 1.01 (OSH) and the LAI-based SLA coefficients range from 1.007 (WSV) to 1.076 (EBF), confirming the consistency in fPAR, LAI values between MOD15A2H and VNP15A2H (Xu et al., 2018; Yan et al., 2021).

## 2.5 Global Boundary Conditions

To verify that global carbon use efficiency (CUE), or NPP:GPP ratios, are reasonable, we conducted global simulations of GPP and NPP using the re-calibrated BPLUT. To overcome resource limitations, global simulations were conducted at 5-km scale from 2000-2021 (for MODIS) or 2012-2021 (for VIIRS). This approach is similar to previous MOD17 global simulations conducted at 1-degree resolution (Zhao et al., 2005). The global 5-km dominant PFT is defined as the majority land-cover type within a 5-km window over the MODIS MCD12Q1 (500-m) grid. We then created gap-filled 5-km fPAR and LAI time series using the approach of Zhao et al. (2005); the gap filling addresses data gaps from either cloud contamination or missing data during non-retrieval periods due to lower solar altitude at high latitudes during winter. Based on these 5-km, multi-year runs, the average annual GPP, NPP, and CUE were calculated within each PFT group.

## 2.6 Model Validation

Some GPP data were withheld during model calibration. For most PFTs, between 20 and 25 site-years of (daily) EC flux tower data, for up to 5 different tower sites, were reserved for validation. Because there are few sites where the majority of land-cover pixels are MF, GRS, DNF, or CSH, only 15 site-years are used for MF and GRS canopies and only 4 site-years are used for DNF and CSH. Each site-year reserved had valid data on at least 97% of data-days, ensuring that nearly complete years were used. Any missing days (3% or less) were interpolated by forward-backward filling to ensure an annual total based on 365 days.

For NPP model validation, because of the dearth of reliable NPP measurements, we used a 3-fold cross-validation to simultaneously estimate best-fit parameters and goodness-of-fit. In combination with MCMC, this means that a random subset of the NPP measurements was reserved in each fold and that nine chains (three folds times three chains in each fold) were obtained. Chains within a fold were pooled and the posterior mean parameters were used to calculate the goodness-of-fit, including bias, root mean-squared error (RMSE), and Pearson’s correlation. These metrics were then averaged across folds to obtain the final goodness-of-fit values.

Three official MOD17 products were validated: MOD17A2H daily GPP, MOD17A3H annual GPP, and MOD17A3H annual NPP. Validation metrics include RMSE, normalized RMSE (nRMSE), unbiased RMSE, and Pearson’s correlation coefficient; these were computed for products based on the MOD17 C61 BPLUT, updated MOD17 BPLUT and new VNP17 BPLUT. For MOD17A2H, daily tower GPP fluxes were aggregated (summed) to 8-day intervals matching the MOD17A2H 8-day GPP. For MOD17A3H annual GPP, because there are so few towers with valid data for at least 97% of days per year, we did not use the reserved validation sites only; instead, all tower sites with valid data were

318 used. This may overestimate the accuracy of the updated annual GPP product, since  
 319 the annual GPP validation dataset includes several data points used in calibration.

320 We also validated MOD17 and VNP17 interannual NPP predictions against one  
 321 top-down and three bottom-up estimates of global, annual NPP. First, the 2020 Global  
 322 Carbon Budget (Friedlingstein et al., 2020) provides mean monthly NEE (2000-2016)  
 323 based on atmospheric inversion on a 1-degree global, equirectangular grid. We calculated  
 324 total annual NEE from these data and then resampled them onto a 0.5-degree grid to  
 325 combine with global, up-scaled estimates of  $R_H$  from X. Tang et al. (2020); NPP is then  
 326 calculated as  $R_H - \text{NEE}$  (“GCB2020”). Second, we estimated total annual NPP (2000-  
 327 2017) from the TRENDYv7 ensemble mean monthly GPP and  $R_A$  fields (Le Quéré et  
 328 al., 2018; Sitch et al., 2015), on a 1-degree grid. Third, the ensemble mean NPP (2000-  
 329 2010) from MsTMIP (BG1 simulation), on a 0.5-degree grid, was used as another bottom-  
 330 up estimate (Huntzinger et al., 2013). Fourth, the up-scaled flux-tower estimates from  
 331 FLUXCOM, driven by remote sensing and surface meteorological data (“RS+METEO”),  
 332 were also compared, based on driver data from ERA5 (Jung et al., 2020). These inde-  
 333 pendent estimates were compared to MOD17 and VNP17 annual NPP and their corre-  
 334 spondence quantified by RMSE and Pearson’s correlation coefficient.

335 To compute global annual fluxes from the independent GCB2020, TRENDYv7, MsT-  
 336 MIP, and FLUXCOM datasets, given their coarse spatial resolution and lack of equal-  
 337 area projection, we projected the annual data onto a 9-km Equal-Area Scalable Earth  
 338 Grid (EASE-Grid 2.0) using nearest-neighbor resampling. Then, after masking the data  
 339 to a similarly resampled MCD12Q1 land area map, totaled the flux densities after scal-  
 340 ing each pixel by its land area. This may result in slightly different estimates than re-  
 341 ported in the literature for these products, but was ultimately necessary as those pub-  
 342 lications do not always report annual flux estimates.

## 343 2.7 Uncertainty Analysis

344 To quantify uncertainty in MOD17 GPP estimates, we applied error propagation  
 345 by computing the Jacobian,  $J$ , of the GPP model with respect to fPAR and  $\varepsilon_{\max}$ , sep-  
 346 arately, for each PFT. The variance in GPP due to model inputs or parameters  $\theta$  is given:

$$347 \sigma_{\text{GPP}}^2(\theta) = J_\theta C J_\theta^T \quad (3)$$

348 where  $C$  is the error covariance matrix. To quantify the separate contributions of  
 349 fPAR and  $\varepsilon_{\max}$ , this equation reduces to a scalar product, where  $C$  is the error in fPAR  
 350 or  $\varepsilon_{\max}$ . We focused on fPAR and  $\varepsilon_{\max}$  because the error in these parameters is known.  
 351 fPAR error is given as 10 fPAR units (Myneni, 2018) and the standard error in the  $\varepsilon_{\max}$   
 352 posterior is assumed to be representative. To facilitate uncertainty quantification, we also  
 353 assume that errors in fPAR and  $\varepsilon_{\max}$  are uncorrelated. We used Gaussian error prop-  
 354 agation to estimate the uncertainty in annual GPP due to the compensating errors in  
 355 daily GPP estimates. Overall uncertainty was calculated by pooling data for all PFTs,  
 356 using only the GPP validation data, which effectively stratifies the data so approximately  
 357 equal site-days are included from each PFT.

358 To quantify uncertainty in MOD17 annual NPP estimates, we use a Monte Carlo  
 359 approach because it is much more difficult to compute partial derivatives of the NPP  
 360 model. We repeatedly sampled from the posterior NPP parameters, with replacement,  
 361 calculating the RMSE in mean annual NPP based on the Cal-Val dataset. The coeffi-  
 362 cient of variation in RMSE is then reported, separately, for each PFT.

## 363 3 Results

364 The Sobol’ sensitivity analysis indicates that more than 80% of the variance in the  
 365 GPP model is determined by the  $\varepsilon_{\max}$  parameter alone (Figure 2). The upper bounds

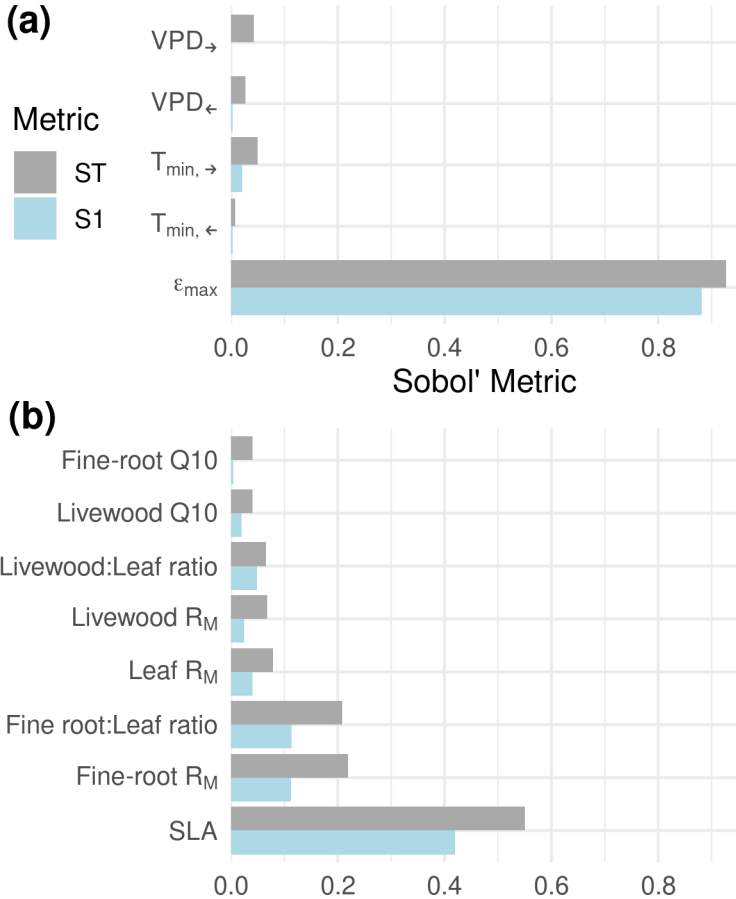


Figure 2: Sobol' sensitivity metrics for the MOD17 GPP (a) and NPP (b) models. The direct effect of the parameter on model estimates is indicated by S1; the total effect (including higher-order interactions) is indicated by ST.  $T_{\min,\leftarrow}$  and  $VPD_{\leftarrow}$  refer to the lower (left-hand) bounds of minimum temperature and VPD; the left-hand bound is the temperature (VPD) at which photosynthesis is completely limited (unlimited) by temperature (VPD).  $T_{\min,\rightarrow}$  and  $VPD_{\rightarrow}$  refer to the upper (right-hand) bounds of minimum temperature and VPD; the right-hand bound is the temperature (VPD) at which photosynthesis is completely unlimited (limited) by temperature (VPD).

of the environmental constraints,  $T_{\min,\rightarrow}$  and  $VPD_{\rightarrow}$ , are more important than the lower bounds and have weak, second-order effects through  $\varepsilon_{\max}$ . The annual NPP model has a strong direct effect of SLA (42%) but also moderately strong total effects from the fine root-leaf ratio (`froot_leaf_ratio`) and base  $R_M$  for fine roots. These sensitivities are partly reflected in the model-data fusion results. In the GPP calibration, the posterior distributions for the environmental scalars are fairly flat, resembling the uniform priors and indicating that the observed GPP data are consistent with a wide range of thresholds for  $T_{\min}$  and VPD. Similarly, the `Q10_livewood` mean *a posteriori* estimate was close to the prior mean for most PFTs.

### 375      3.1 Optimal Parameters for BPLUT

376      The posterior distributions were compared to the C61 BPLUT and the wider literature,  
 377      assessing both consistency with the previous product and realism. As an additional  
 378      boundary condition, the mean global CUE values for each PFT were expected to  
 379      be close to 0.46 (Collalti & Prentice, 2019) and much lower for EBF (Malhi, 2012). Dur-  
 380      ing NPP calibration, to ensure realism in the BPLUT values and the simulated, global  
 381      CUE values, we rejected some of the mean *a posteriori* (MAP) estimates after calibra-  
 382      tion. When the MAP was rejected, it was replaced either by the prior mean for that PFT  
 383      (Table S7) or by the MAP of a similar PFT. The updated MOD17 BPLUT and new VNP17  
 384      BPLUT can be found in the Supplement (Tables S9, S10).

385      Given the low sensitivity of the GPP model to the lower bounds of the environ-  
 386      mental scalars (Figure 2), we opted to fix these at their C61 values; upper bounds re-  
 387      mained free parameters during MOD17 calibration. The  $\text{VPD}_{\rightarrow}$  posterior likelihood in-  
 388      creased rapidly with VPD but, above ca. 3000 Pa the posterior flattens out. The  $T_{\min,\rightarrow}$   
 389      posteriors are more complex, with most PFTs showing little sensitivity to this param-  
 390      eter. Consequently, the optimal values for both  $\text{VPD}_{\rightarrow}$  and  $T_{\min,\rightarrow}$  were chosen as the  
 391      maximum *a posteriori* estimate, as the mean (or median), given a uniform prior, tends  
 392      to fall near the middle of the prior bounds. The  $\varepsilon_{\max}$  posteriors were symmetric and the  
 393      prior mean was within the interquartile range (IQR) for all PFTs. The results are con-  
 394      sistent with Madani et al. (2017), but the optimal  $\varepsilon_{\max}$  appears to be significantly lower  
 395      than its C61 value for shrublands and savannas, higher for croplands, and otherwise sim-  
 396      ilar to C61 (Figure S9).

397      Consistent with the literature, the livewood Q10 posterior is narrow and resembles  
 398      the prior. The fine-root Q10 posterior varies widely among PFTs, which is partly a re-  
 399      flection of the uncertainty in the literature. Deciduous canopies and Mixed Forest have  
 400      the highest Q10\_froot values. As Q10\_froot is not likely to be less than 1.0 (Atkin et  
 401      al., 2000), the posterior was rejected in favor of the prior in such cases. Posterior  $R_M$   
 402      for leaves and fine roots were generally lower than the prior means from TRY but within  
 403      the range of the C61 BPLUT. The NPP data indicate that the optimal leaf  $R_M$  rate com-  
 404      pares well with C61 for woody forest PFTs; however, posterior means for other PFTs were  
 405      higher than the C61 value and close to the prior mean. The fine-root  $R_M$  posteriors vary  
 406      widely and few are close to their C61 values. The posterior livewood  $R_M$ , however, com-  
 407      pares well with the C61 BPLUT and the prior mean, except for EBF and shrublands,  
 408      where it is significantly higher. The `livewood_mr_base` prior mean for EBF was used  
 409      in place of the MAP.

### 410      3.2 Validation against Tower Fluxes and Field Data

411      The C61 annual GPP (MOD17A3H) estimates compare well with tower annual GPP  
 412      among those sites with nearly complete years (Table 4). Under-estimation of GPP is ap-  
 413      parent for ENF, but C61 also over-estimates GPP in medium-productivity EBF (Table  
 414      S11). C61 GPP performs best in ENF, EBF, and GRS (nRMSE within 13-17%) but most  
 415      severely under-estimates GPP in ENF and MF (nRMSE  $\geq$  49%). C61 8-day GPP (MOD17A2H),  
 416      divided into daily units, indicates the algorithm performs best in shrublands, WSV, and  
 417      GRS (nRSME  $\leq$  7%) and worst in CRO (nRMSE = 26%) because of under-estimation  
 418      (mean bias =  $-1.2 \text{ g C m}^{-2} \text{ day}^{-1}$ ) (Table S13).

419      GPP bias and RMSE were both reduced overall in the Updated product (Table 4),  
 420      with the greatest improvements made at highly productive DBF and CRO sites (Table  
 421      S13). Daily GPP improved for most PFTs, while annual GPP generally improved only  
 422      for herbaceous and forested canopies. High negative bias in annual GPP was significantly  
 423      reduced for ENF, GRS, and CRO (-196, -174 and  $-9 \text{ g C m}^{-2} \text{ year}^{-1}$  after recalibration,  
 424      respectively). C61 MOD17 generally under-estimates GPP, particularly at high mag-  
 425      nitudes (Heinsch et al., 2006; Y. Zhang et al., 2008), and slightly over-estimates annual

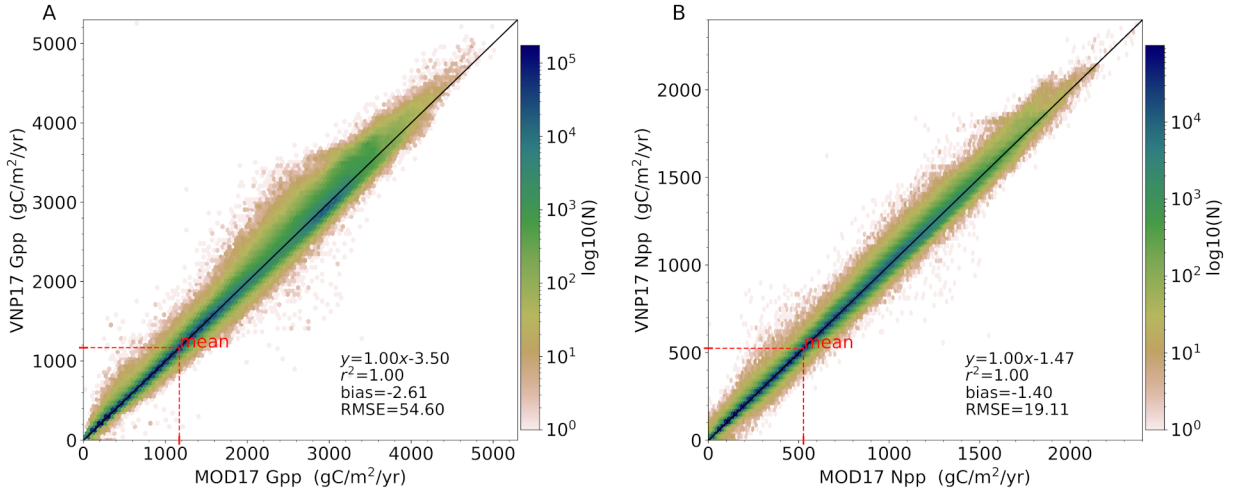


Figure 3: Comparison of mean annual GPP (left) and NPP (right) from the overlapping 10-year period for MODIS MOD17 and VIIRS VNP17 (2012-2021), based on global, 5-km simulations.

NPP, particularly in forested areas (Table S15). After re-calibration, GPP bias is reduced but is systematically similar to C61, while NPP bias is almost eliminated in individual PFTs, save for ENF, which has a strong, negative mean bias (Table S15). This also leads to an overall negative bias in the updated product (Table 4).

Annual NPP skill is improved in the MOD17 update, compared to C61 (Table 4, Figures S10-S11). C61 Annual NPP (MOD17A3H) performs best in shrublands, savannas, and herbaceous canopies ( $nRMSE \leq 17$  percent) and this pattern is similar for the updated product, though DNF, DBF, and MF are also considerably improved (Table S15). The magnitude of annual NPP RMSE in C terms is small ( $\sim 0.7 \text{ g C m}^{-2} \text{ day}^{-1}$ ) but performance varies widely by PFT, with the greatest nRMSE values in forest canopies. In the update, spatial correlation in annual NPP is improved for all PFTs ( $\geq 0.5$ ) except ENF. Annual NPP RMSE was also improved for all PFTs, except ENF.

Plant CUE (NPP:GPP ratio) is an emergent property of ecosystems simulated by MOD17. When the new annual GPP and NPP products are combined, we find that the BPLUT updates lead to substantial changes in CUE from C61. In terms of agreement with the MsTMIP ensemble, the updates improve plant CUE for all PFTs except DNF, SAV, and GRS (Figure S12). When compared to the measured CUE values compiled by Collatti and Prentice (2019) for woody plants, the updates improve plant CUE for all PFTs except EBF (Figure S13), for which median CUE is 0.49 (0.40 in MsTMIP ensemble, 0.44 in C61, and 0.37 in the update).

At global extent, the new VNP17 annual GPP and NPP products are very similar to the updated MOD17 products (Figure 3). The new VIIRS VNP17 BPLUT was used in the same validation scheme as for MOD17 GPP and NPP. However, because VIIRS fPAR and LAI data are only available starting in 2012 and many FLUXNET sites do not report data after 2012, there are far fewer site-weeks or site-years to use for validating VNP17 daily GPP than for MOD17. In particular, majority-DNF sites are not represented in the 2012-2017 period and no majority-DBF sites have years with at least 97% of valid data-days within this span. When using a common validation data mask, it is apparent that the VNP17 BPLUT produces daily GPP estimates quite similar to the updated MOD17 BPLUT (Table 4), except that VNP17 shows potential degra-

Table 4: Validation statistics for the daily MOD17A2H/VNP17A2 GPP and annual MOD17A3H/VNP17A3 GPP and NPP products, as compared to EC flux tower and NPP cross-validation (Cal-Val) data, respectively. For daily GPP validation, daily tower GPP and updated simulations were aggregated to 8-day periods to match MOD17A2H. For annual GPP validation, all tower data were used instead of only reserved data. The normalized RMSE (%) is based on the overall observed range of daily GPP or annual NPP. The largest valid tower GPP observation was  $20.4 \text{ g C m}^{-2} \text{ day}^{-1}$ . The largest NPP flux in the NPP Cal-Val dataset was  $1,922 \text{ g C m}^{-2} \text{ year}^{-1}$  (nRMSE for annual NPP is the cross-validation mean). 8-day GPP was evaluated for the entire FLUXNET record (2000-2017) but also on a common, reserved test dataset from 2012-2017, for compatibility with VHIIRS; the latter case does not include any results from DNF due to missing FLUXNET data in this period. \*VNP17 Annual GPP validation does not include DNF or DBF canopy, as none of the FLUXNET sites have any year with at least 97% of valid data-days during the period 2012-2017.

Model	Bias (g C m <sup>-2</sup> )	RMSE (g C m <sup>-2</sup> )	ubRMSE (g C m <sup>-2</sup> )	nRMSE (%)	<i>r</i>
MOD17 8-day GPP (C61), 2000-2017	-4.04 day <sup>-1</sup>	2.69 day <sup>-1</sup>	2.41 day <sup>-1</sup>	13.7%	0.79
MOD17 8-day GPP (Update), 2000-2017	-2.77 day <sup>-1</sup>	2.34 day <sup>-1</sup>	2.07 day <sup>-1</sup>	12.0%	0.84
MOD17 8-day GPP (C61), 2012-2017	-2.56 day <sup>-1</sup>	2.25 day <sup>-1</sup>	1.82 day <sup>-1</sup>	11.0%	0.81
MOD17 8-day GPP (Update), 2012-2017	-2.06 day <sup>-1</sup>	2.16 day <sup>-1</sup>	1.72 day <sup>-1</sup>	10.6%	0.82
VNP17 8-day GPP, 2012-2017	-1.75 day <sup>-1</sup>	2.17 day <sup>-1</sup>	1.72 day <sup>-1</sup>	10.6%	0.82
MOD17 Annual GPP (C61)	-266 year <sup>-1</sup>	546 year <sup>-1</sup>	n.a.	14.4%	0.78
MOD17 Annual GPP (Update)	-210 year <sup>-1</sup>	504 year <sup>-1</sup>	n.a.	13.3%	0.80
VNP17 Annual GPP*	-179 year <sup>-1</sup>	523 year <sup>-1</sup>	n.a.	14.0%	0.82
MOD17 Annual NPP (C61)	9 year <sup>-1</sup>	297 year <sup>-1</sup>	n.a.	16.0%	0.49
MOD17 Annual NPP (Update)	-59 year <sup>-1</sup>	261 year <sup>-1</sup>	n.a.	14.1%	0.51
VNP17 Annual NPP	-46 year <sup>-1</sup>	274 year <sup>-1</sup>	n.a.	14.8%	0.49

456 tion in MF and improvement in OSH and a less-negative overall bias (Tables S13, S14).  
 457 VNP17 annual NPP estimates, however, are generally less accurate than for MOD17,  
 458 with particularly high RMSE in ENF, OSH, WSV, and SAV compared to the updated  
 459 MOD17 (Tables S15, S16). Compared to the statistics in Table 4, when the longer val-  
 460 idation record available to MODIS MOD17 is used instead, there is a more substantial  
 461 improvement over C61 in daily GPP RMSE ( $2.69 \text{ g C m}^{-2} \text{ day}^{-1}$  for C61 versus  $2.34$   
 462 for the Updated BPLUT) and correlation (0.77 for C61 versus 0.84 for the Updated BPLUT).

Table 5: Root-mean squared difference (RMSD) in annual NPP ( $\text{g C m}^{-2} \text{ year}^{-1}$ ) at FLUXNET sites for each product, compared to independent NPP datasets.

NPP Dataset	C61	MOD17 Update	New VNP17
Global Carbon Budget (2000-2016)	341	272	276
TRENDYv7 Ensemble (2000-2017)	331	327	289
MsTMIP Ensemble (2000-2010)	341	313	n.a.

463 Compared to the independent NPP estimates at FLUXNET sites from bottom-up  
 464 and top-down approaches, the updated MOD17 and VNP17 products also show substan-  
 465 tial reductions in annual NPP RMSE over C61 (Table 5); again, VNP17 is very similar  
 466 to MOD17 in this respect (Table S17). When broken out by PFT (Tables S18-S20), it's  
 467 clear the updated MOD17 has improved skill in annual NPP for some of the most pro-  
 468 ductive PFTs: EBF (C61 mean RMSE=  $717 \text{ g C m}^{-2} \text{ year}^{-1}$ , updated MOD17 mean  
 469 RMSE= 548 average across independent datasets), DBF (C61 mean RMSE= 247, up-  
 470 dated MOD17 mean RMSE= 195), and CRO (C61 mean RMSE= 304, updated MOD17  
 471 mean RMSE= 272). Most importantly, the overall GPP and NPP magnitudes are very  
 472 similar between VNP17 and the updated MOD17 (Figure 3).

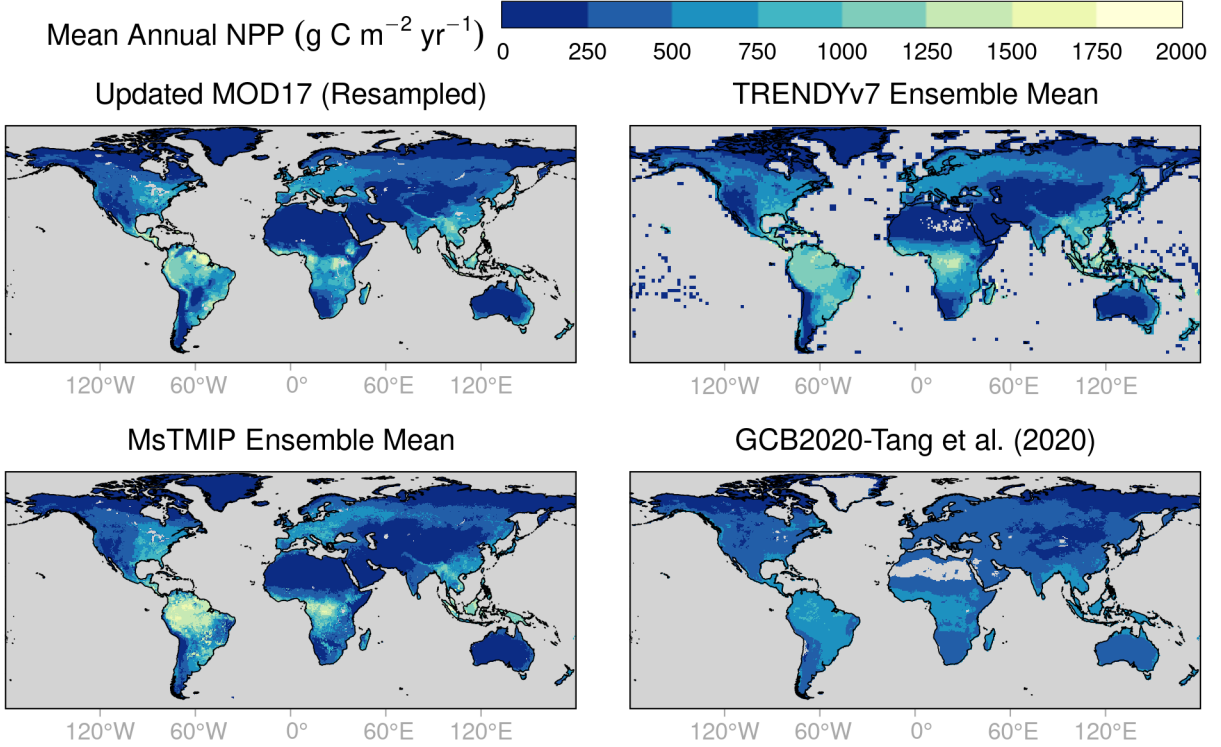


Figure 4: Comparison of mean annual NPP (2000-2010) across four products: the updated MOD17 product, based on the 5-km global simulation and resampled to 0.5-degrees; the TRENDYv7 ensemble mean, at 1-degree resolution; the MsTMIP ensemble mean at 0.5-degrees; and the synthetic NPP estimate from the 2020 Global Carbon Budget and Tang et al. (2020). In the MOD17 image, land areas not simulated in MOD17 (e.g., barren lands) are filled with zero annual NPP.

473

### 3.3 Mean, Trend, and Interannual Variability

474  
475  
476  
477  
478  
479  
480  
481

The mean global GPP flux (2000-2018) in the updated MOD17 product is  $127 \pm 2.8 \text{ Pg C year}^{-1}$ , which compares well with that of the TRENDYv7 ensemble mean over the same period ( $126 \pm 2.4 \text{ Pg C year}^{-1}$ ), and is an increase over the estimate from C61 ( $119 \pm 2.9 \text{ Pg C year}^{-1}$ ). If we consider the period 2012-2018, mean global GPP flux from the new VNP17 is quite similar to the updated MOD17 estimate,  $129.6 \pm 1.7$  versus  $129.7 \pm 1.7 \text{ Pg C year}^{-1}$ , and both are higher than the C61 estimate over the same period ( $121.6 \pm 1.6 \text{ Pg C year}^{-1}$ ). Mean global NPP flux from the new products over 2012-2018 is  $58.4 - 58.5 \pm 1.1 \text{ Pg C year}^{-1}$ , compared to  $60.7 \pm 1.1$  in C61 (Table S21).

482  
483  
484  
485  
486  
487  
488  
489  
490

The updated MOD17 and new VNP17 annual NPP estimates exhibit strong spatial correlation (Figures 4, 5, and S14-S16) with bottom-up estimates from the TRENDYv7 (MOD17  $r = 0.85$ , VNP17  $r = 0.86$ ) and MsTMIP ensembles (MOD17  $r = 0.79$ ) and also compares well with the top-down, global synthesis of NPP based on the Global Carbon Budget (MOD17 and VNP17  $r = 0.71$ ). Annual GPP estimates from both products show even stronger spatial correlations with TRENDYv7 (MOD17 and VNP17  $r = 0.91$ ). In terms of global, interannual NPP and  $R_A$  variability, MOD17 compares very well to the TRENDYv7 and MsTMIP ensembles, with the vast majority of the global land domain exhibiting strong, positive correlations (Figure S17); VNP17 IAV is very

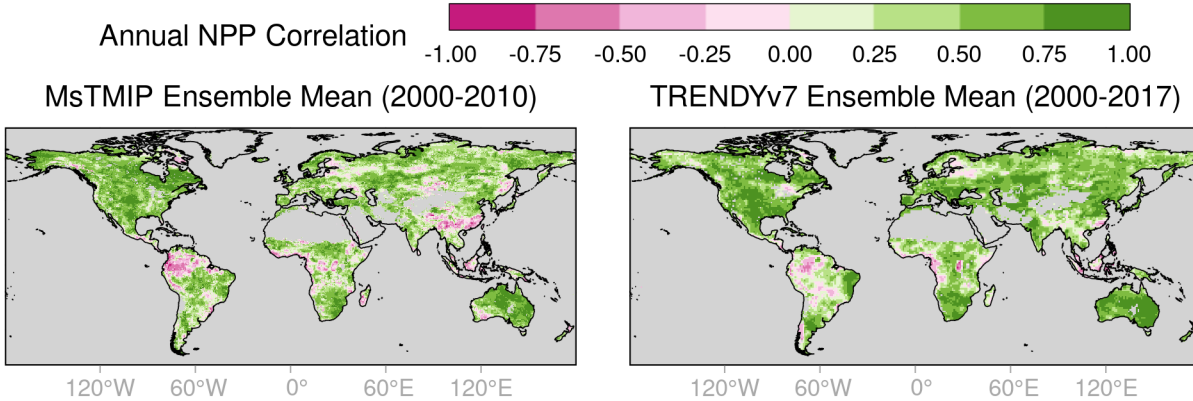


Figure 5: Comparison of interannual correlation in NPP between the updated MOD17 product (based on the 5-km global simulation) and the MsTMIP ensemble mean at 0.5-degrees or the TRENDYv7 ensemble mean at 1-degree resolution. The MOD17 product was resampled to match either product.

similar to that of MOD17 (Figures S18-S21). Negative correlations are found mainly in humid, tropical regions where IAV is low and persistent cloud cover leads to more reliance on fPAR climatology.

We also compared MOD17 C61 and the updated MOD17 to the MsTMIP and TRENDYv7 ensemble means in terms of interannual variation (IAV) in GPP and NPP (Figure 6). All products show a significant, upward trend, based on Theil-Sen median trend estimates. MOD17 C61 and the updated MOD17 display increasing GPP (NPP) trends of 0.45 and 0.47 (0.27 and 0.25) Pg C year<sup>-2</sup>, respectively, over 2000-2018 compared with 0.41 (0.21) Pg C year<sup>-2</sup> for the TRENDYv7 ensemble means. Trends are lower in the period 2012-2021; for MOD17 C61, the updated MOD17, and the new VNP17 we find GPP (NPP) trends of 0.38, 0.44, and 0.35 (0.17, 0.13, 0.11) Pg C year<sup>-2</sup>. For the unified period of 2000-2010 (VNP17 drops out), both MOD17 products show greater IAV in GPP and NPP than MsTMIP and TRENDYv7. The IAV is slightly lower in the updated MOD17 compared to C61, which may reflect the bias-variance trade-off, i.e., a tendency in model calibration toward a narrower range of parameter variability.

### 3.4 Uncertainty Analysis

The error propagation indicates that a substantial portion of the error in daily and annual GPP estimates comes from error in fPAR (Tables S22, S23); at least 1.0 g C m<sup>-2</sup> day<sup>-1</sup> for all PFTs and greater than 1.5 g C m<sup>-2</sup> day<sup>-1</sup> for most. Uncertainty in  $\varepsilon_{\max}$  is a negligible part of the error in GPP estimates, accounting for less than 0.12 g C m<sup>-2</sup> day<sup>-1</sup> in both MOD17 and VNP17, though with the greatest impact on EBF. The magnitude of the fPAR error contribution is generally proportional to the total error by PFT.

The error budget for annual NPP estimates generally corresponds to the sensitivity analysis: uncertainty in SLA is usually the largest source of error in NPP estimates, among free parameters (Tables S24, S25). However, some PFTs have large error contributions from other parameters. Uncertainty in Q10\_froot is a major contributor to uncertainty in annual NPP for both ENF and EBF and the greatest contributor for CRO. Uncertainty in froot\_mr\_base is a major source of uncertainty in ENF and GRS, while uncertainty in leaf\_mr\_base is a major source for WSV. Uncertainty in SLA has surprisingly little impact on annual NPP estimates in shrublands; no model parameters an-

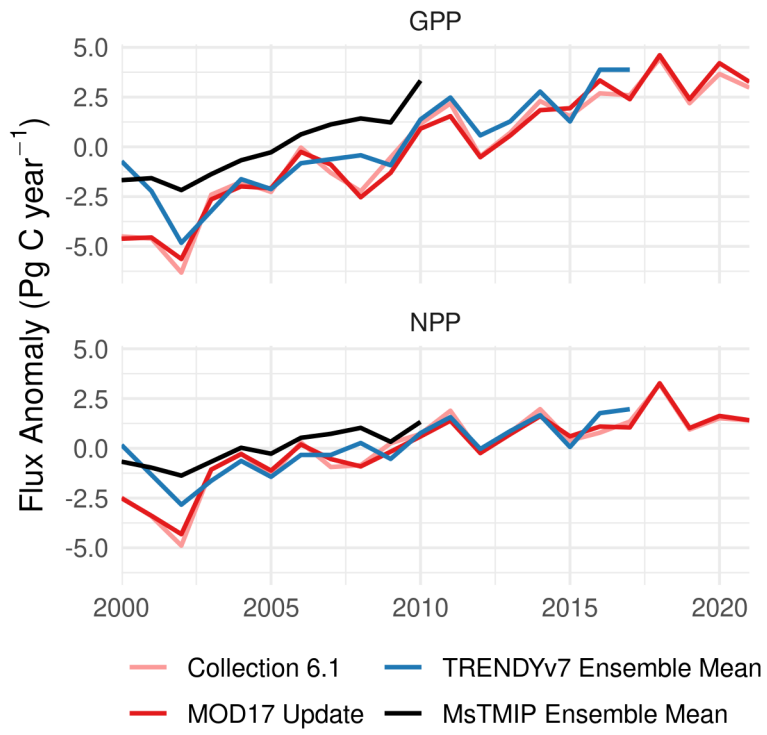


Figure 6: Interannual variation (IAV) in GPP, NPP (annual flux minus interannual mean) for the MOD17 products, shown alongside that of the Multi-Scale Synthesis and Terrestrial Model Intercomparison Project (MsTMIP) and TRENDYv7 ensemble means.

521 analyzed here contributed major uncertainty to estimates for this PFT, which is found pre-  
 522 dominantly at high latitudes.

## 523 4 Discussion

524 Prudent use of models requires that they are regularly evaluated, checking both  
 525 the model predictions (validation) and assumptions (verification) against independent  
 526 data. MOD17 is a good candidate for continued use in the VIIRS era, but requires val-  
 527 idation and verification to contextualize its estimates of ecosystem productivity. Here,  
 528 independent data on plant traits have been combined with GPP and NPP measurements  
 529 from flux towers and field surveys to improve both the accuracy and the realism of MOD17.

### 530 4.1 Inferring the Optimal Biome Properties

531 Retrospectively, plant trait data from TRY and the literature allow for a qualita-  
 532 tive validation of the MOD17 Collection 6.1 (C61) BPLUT. We found that maximum  
 533 LUE ( $\varepsilon_{\max}$ ) compared well to the global optimum LUE defined by Madani et al. (2017)  
 534 for most PFTs, but C61  $\varepsilon_{\max}$  is likely too high for shrubland and savanna, and too low  
 535 for croplands (Gan et al., 2021). Some studies have suggested higher  $\varepsilon_{\max}$  in ENF (Coops  
 536 et al., 2007) and in shrublands (J. Chen et al., 2014) while others find, as indicated here,  
 537 it should be lower (Yuan et al., 2014; Madani et al., 2017). Previous generations of the  
 538 MOD17 BPLUT used a comparatively small number of EC towers (and years of obser-  
 539 vation) in calibration, which may have led to biased  $\varepsilon_{\max}$  estimates. Even among the ex-  
 540 panded FLUXNET collection, there are only five CSH tower sites, three of which are within  
 541 2 km of one another, and all in regions of high aridity. Overall, lower  $\varepsilon_{\max}$  in arid re-  
 542 gions is expected (Garbulsky et al., 2010). This may explain the severe decrease in  $\varepsilon_{\max}$   
 543 for CSH, relative to the C61 BPLUT, which is greater than the corresponding decrease  
 544 in the better-represented OSH canopy.

545 While the TRY database indicates that  $R_M$  for all tissues should be higher than  
 546 that of the C61 BPLUT (Figure S9, Table S7), posterior estimates are generally some-  
 547 where in the middle. Livewood  $R_M$  in C61 is close to that indicated by TRY. SLA in  
 548 the C61 BPLUT also compares well to prior observations from TRY for evergreen and  
 549 herbaceous (GRS and CRO) canopies but is too low otherwise. SLA values from TRY  
 550 may seem high compared to field measurements of SLA (e.g., leaf area per unit leaf dry  
 551 mass) but are consistent with the range of SLA in C terms (leaf area per unit leaf C),  
 552 as the TRY database includes many values above  $100 \text{ m}^2 \text{ kg C}^{-1}$  (Figure S8). Posterior  
 553 SLA values also compare very well to a review by Wright and Westoby (2001).

554 The peculiarities of calibration results for CSH point to a larger issue with MOD17:  
 555 too many poorly defined PFTs. Given that CSH is a tiny proportion (0.2%) of the global  
 556 land surface (Madani et al., 2017), it is reasonable to ask whether this class should be  
 557 combined with OSH in a global “Shrublands” class. This is especially salient in light of  
 558 evidence that multiple PFTs may be over-differentiated (Yuan et al., 2014) and that en-  
 559 vironmental filtering (Funk et al., 2017) may lead to more robust plant response than  
 560 static and somewhat arbitrary functional types (Y. Liu et al., 2021). One practical con-  
 561 sequence is that the prior mean for SLA in both OSH and CSH may be too high, as in-  
 562 dicated by the low posterior  $R_M$  rates in these PFTs.

563 Our uncertainty analysis of the NPP sub-model largely follows the sensitivity anal-  
 564 ysis but also emphasizes where parameters could be better constrained. SLA is the most  
 565 important parameter for NPP estimation in MOD17 as, despite its relatively high cer-  
 566 tainty (Figure S9, based on prior information from TRY), it has the greatest impact on  
 567 NPP error. Leaf properties in croplands are particularly uncertain (Figure S22), likely  
 568 due to the wide variety of global crop types. Future LUE models like MOD17 might ben-

569 fit from modeling SLA instead of using a fixed value, given the sensitivity of SLA to  
 570 phenology and environmental conditions (Gong & Gao, 2019; Z. Liu et al., 2022).

## 571 4.2 Performance of Global GPP and NPP Products

572 Relative to C61, model-data fusion lead to improvements in 8-day and annual GPP  
 573 and annual NPP flux estimates, based on reserved EC tower data, NPP cross-validation  
 574 with field data, and independent bottom-up and top-down NPP estimates. Since 2012,  
 575 the persistent negative GPP bias of MOD17 was reduced by at least  $0.5 \text{ g C m}^{-2} \text{ day}^{-1}$   
 576 and by over  $50 \text{ g C m}^{-2} \text{ year}^{-1}$ ; over a longer record, bias was reduced by more than  
 577 twice as much (Table 4). These improvements put the updated MOD17 and new VNP17  
 578 8-day GPP product on par with other data-driven approaches combining satellite and  
 579 flux-tower data (Joiner et al., 2018). Global annual GPP flux estimates in the new prod-  
 580 ucts (mean 2012-2021 annual GPP flux of  $130 \pm 1.5 \text{ Pg C year}^{-1}$ ) are higher than the  
 581 estimates of C61 ( $122 \pm 1.4 \text{ Pg C year}^{-1}$ ) and other satellite-based estimates but are more  
 582 in line with oxygen isotope studies (Welp et al., 2011), recent syntheses (J. M. Chen et  
 583 al., 2012; Piao et al., 2013; Anav et al., 2015) (Figure 7), and bottom-up studies (Madani  
 584 et al., 2018, 2020), particularly for years since 2012 (Y. Zhang, Xiao, et al., 2017). The  
 585 new GPP estimates also agree better with TRENDYv7 ( $128.6 \pm 1.4$  for 2012-2021).

586 Annual NPP skill (nRMSE) was improved by almost 2 percentage points, a reduc-  
 587 tion in RMSE of about  $30 \text{ g C m}^{-2} \text{ year}^{-1}$ . The updated and new products' reduction  
 588 in global annual NPP flux ( $58.4\text{--}58.6 \pm 0.9 \text{ Pg C year}^{-1}$  for 2012-2021) is more consis-  
 589 tent with estimates from the MsTMIP ensemble and combined results from the Global  
 590 Carbon Budget (2020) and up-scaled soil respiration data (X. Tang et al., 2020); it's also  
 591 closer than C61 to the estimate from the meta-analysis by Ito (2011) ( $56.2 \pm 14.3 \text{ Pg C}$   
 592  $\text{year}^{-1}$ ). However, the mean annual NPP flux from the TRENDYv7 ensemble mean is  
 593 higher and closer to the original estimate of MOD17 C61 (Table S21), as is the median  
 594 of the spread in TRENDYv7 models (Figure 7). The inter-model spread of TRENDYv7  
 595 and earlier syntheses (Cramer et al., 1999; Ito, 2011) suggests persistent high uncertainty  
 596 in any model's representation of terrestrial NPP. It also suggests at least the possibil-  
 597 ity that the field estimates of NPP used here (Table 3) may not be too large, despite con-  
 598 cerns about their reliability and representativeness (Clark et al., 2001; Zhao et al., 2006).

599 The greatest strength of the MOD17 and VNP17 products is their long period of  
 600 record, allowing an examination of interannual variability and trends. The strong increase  
 601 in NPP observed over 2000-2010 (Figure 6) is inconsistent with the report of a reduc-  
 602 tion in NPP by Zhao and Running (2010). This could be attributed to a difference in  
 603 the climate drivers used in different versions of MOD17 and the sensitivity of GPP to  
 604 prevailing weather conditions (Zhao et al., 2006). The 1-km estimates of MOD17 Col-  
 605 lection 5.1, from 2000 to 2015, used by Zhao and Running (2010) were driven by NCEP  
 606 reanalysis data (Kanamitsu et al., 2002) whereas the operational MOD17 (and future  
 607 VNP17) products use GMAO data; these differences have led to different anomalies in  
 608 GPP and NPP (Zhao et al., 2005). The uncertainty in LUE models like MOD17 due to  
 609 climate drivers merits further exploration.

610 However, even after recalibration, MOD17 and the new VNP17 GPP products still  
 611 show large negative biases (Table 4). Previous studies have established that MOD17 gen-  
 612 erally under-estimates GPP (Heinsch et al., 2006; Coops et al., 2007; Propastin et al.,  
 613 2012; Sjöström et al., 2013; J. Chen et al., 2014; Huang et al., 2018), especially in grass-  
 614 lands (Zhu et al., 2018) and in highly productive regions (Wang & Ogawa, 2017), and  
 615 that this may be explained by a failure to account for diffuse PAR (Guan et al., 2022).  
 616 Although it has been suggested that  $\varepsilon_{\max}$  should be increased (Wang & Ogawa, 2017;  
 617 Huang et al., 2018), this model-data fusion is consistent with the previous global anal-  
 618 ysis of Madani et al. (2017) indicating that  $\varepsilon_{\max}$  should be *decreased* for low-productivity  
 619 shrublands and savannas and *increased* in DBF, MF, and croplands, relative to C61. This

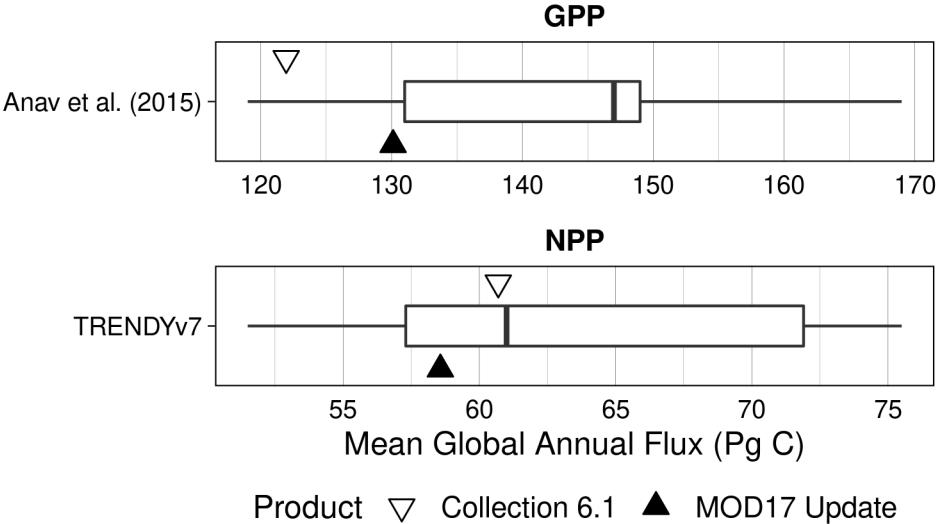


Figure 7: Comparison of MOD17 and VNP17 annual GPP and NPP fluxes with estimates from different models, as synthesized by Anav et al. (2015), for GPP, or represented by the inter-model spread of NPP estimates from the TRENDYv7 ensemble.

may reflect subsequent improvements in the gap-filled MOD15A2HGF fPAR and LAI data. Notably, the updated MOD17 and new VNP17 BPLUT both substantially reduced the negative bias in croplands, which was found to be severe in Collection 6 (Huang et al., 2018).

Annual NPP estimates were improved, over C61, to a greater degree than 8-day or annual GPP estimates (reduction in nRMSE of 0.4-1.0% for GPP but 1.2-1.9% for NPP), likely because there are more parameters to optimize in the NPP model. However, in the updated MOD17 and new VNP17 products, there is a large negative bias in ENF, likely introduced when fine-root  $R_M$  was increased to reduce the spuriously high CUE that emerged from global simulations. Leaf  $R_M$  and SLA (based on prior information from hundreds of species in TRY) are already both low for this PFT and the cross-validation RMSE is very low (compared to other PFTs); consequently, there are few options to mitigate this bias and avoid unrealistically high CUE values. The simultaneous improvement in annual NPP RMSE but decline in correlation likely reflects the sensitivity of NPP to local conditions that may not be adequately reflected by the 11 PFTs used in MOD17.

Another source of NPP variability is the variation in plant traits (and BPLUT parameters) themselves, over time and along environmental gradients, which is currently not reflected in the MOD17 model structure. SLA has been shown to vary with moisture and nutrient availability (Dwyer et al., 2014), and the spatial and temporal variation in SLA, if accounted for, might reduce estimated NPP magnitudes (Verheijen et al., 2015). It has also been established that fine-root respiration is at least partly coupled with canopy photosynthetic uptake (Högberg et al., 2001; Drake et al., 2008; Lynch et al., 2013).

How do the new products compare to previous generations? It is difficult to compare to previous performance assessments in carbon units (e.g., RMSE) because the quantity depends on the relative productivity of the EC tower sites included; more produc-

tive sites would generally lead to a higher RMSE. For example, the high RMSE of 8-day GPP in croplands (Table 13) exaggerates the overall RMSE estimated here (Table 4). As an alternative, normalized quantities have been used inconsistently, and while “relative error” (Heinsch et al., 2006) is a common choice, it is also highly sensitive to very low EC tower flux magnitudes. We suggest that only normalized RMSE, relative to the reported range of tower observations, be compared to other assessments. These would suggest that C61 is an improvement over earlier versions and the updated MOD17 BPLUT a further improvement. R. Tang et al. (2015), for example, find Collection 6 annual GPP biases generally twice as large as estimated here for C61, and nRMSE values significantly higher as well, based on less than half as many EC tower sites. Sjöström et al. (2013) found an overall Collection 5.1 GPP RMSE, compared to flux towers in Africa, of  $2.58 \text{ g C m}^{-1} \text{ d}^{-1}$ , higher than our estimate of  $2.25 \text{ g C m}^{-1} \text{ d}^{-1}$  for C61. The performance is sensitive to the driver data used and is generally much better when tower-observed surface meteorology is used (Coops et al., 2007; J. Chen et al., 2014), though some have found otherwise (Wang & Ogawa, 2017).

Error propagation indicates that error in MOD17 and VNP17 GPP estimates is primarily due to error in fPAR retrievals, as in multiple previous studies (Propastin et al., 2012; Fu et al., 2017; Wang & Ogawa, 2017). Given the low sensitivity of these models to environmental scalars, this suggests that dynamic changes in MOD17 modeled GPP are largely a function of changes in canopy extent and vigor, conveyed by changes in fPAR. This feature of LUE models has been an advantage during the EOS era and allowed models like MOD17 to capture trends in the land carbon sink (Figure 6) that are otherwise missed by purely data-driven approaches like FLUXCOM (Yang et al., 2022). And yet, given the modest improvement in the new MOD17 product compared to C61, it's also apparent that the accuracy of these global LUE models is strongly tied to the quality of input datasets, in addition to uncertainty in model parameters and model structure.

## 5 Conclusion

We combined prior information on plant productivity and respiration traits with eddy covariance estimates of GPP and field estimates of NPP for the recalibration of MOD17, the first model to provide global, continuous, weekly estimates of ecosystem productivity. This effort culminated in the final reprocessing of MODIS MOD17 and the development of new VNP17 GPP and NPP products based on VIIRS data. Relative to the current MODIS C61 MOD17 data, the updated MOD17 parameters substantially reduce the negative bias in 8-day GPP, by more than  $1.2 \text{ g C m}^{-2} \text{ day}^{-1}$ ; the RMSE in annual GPP was reduced by  $42 \text{ g C m}^{-2} \text{ year}^{-1}$  and RMSE in annual NPP was reduced by  $36 \text{ g C m}^{-2} \text{ year}^{-1}$  while maintaining or improving global correlations in the spatial pattern of GPP and NPP fluxes.

The combined records of the updated MOD17 and new VNP17 products enable weekly-to-annual terrestrial productivity estimates to be continued through 2030 and beyond. The updated estimates of mean global GPP and NPP for 2012–2021,  $130.1 \pm 1.6$  and  $58.6 \pm 0.9$  (respectively) agree very well with other bottom-up estimates. The long, extant record of MOD17 and VNP17 indicate that terrestrial productivity is increasing over recent decades (2000–2018), with GPP increasing annually by  $0.47 \text{ Pg C year}^{-2}$  and NPP by  $0.25 \text{ Pg C year}^{-2}$ . These trends are supported by independent, bottom-up estimates and all the models examined here do indicate that the rate of increase in GPP and NPP may be slowing down in recent years.

## Open Research Section

The 5-km global simulation outputs (for both MOD17 and the new VNP17) and the driver data required to run, calibrate, and validate MOD17 at FLUXNET sites (with the exception of tower fluxes, which we are not licensed to reproduce) are available at

697 <<https://doi.org/10.5281/zenodo.7682806>>. The repository of the MOD17 algo-  
698 rithm's Python and C source code is available on GitHub at <<https://github.com/arthur-e/MOD17>>.

699 **Acknowledgments**

700 This study was supported by a grant from NASA (NNH20ZDA001N-SNPPSP).

795 **References**

- Anav, A., Friedlingstein, P., Beer, C., Ciais, P., Harper, A., Jones, C., ... Zhao, M. (2015, September). Spatiotemporal patterns of terrestrial gross primary production: A review. *Reviews of Geophysics*, 53(3), 785–818. Retrieved from <http://doi.wiley.com/10.1002/2015RG000483> doi: 10.1002/2015RG000483
- Atkin, O. K., Edwards, E. J., & Loveys, B. R. (2000, July). Response of root respiration to changes in temperature and its relevance to global warming. *New Phytologist*, 147(1), 141–154. Retrieved from <http://doi.wiley.com/10.1046/j.1469-8137.2000.00683.x> doi: 10.1046/j.1469-8137.2000.00683.x
- Bahn, M., Knapp, M., Garajova, Z., Pfahringer, N., & Cernusca, A. (2006, June). Root respiration in temperate mountain grasslands differing in land use. *Global Change Biology*, 12(6), 995–1006. Retrieved 2022-06-27, from <https://onlinelibrary.wiley.com/doi/10.1111/j.1365-2486.2006.01144.x> doi: 10.1111/j.1365-2486.2006.01144.x
- Balch, J. K., Bradley, B. A., Abatzoglou, J. T., Nagy, R. C., Fusco, E. J., & Ma-hood, A. L. (2017, March). Human-started wildfires expand the fire niche across the United States. *Proceedings of the National Academy of Sciences*, 114(11), 2946–2951. Retrieved 2022-07-29, from <https://pnas.org/doi/full/10.1073/pnas.1617394114> doi: 10.1073/pnas.1617394114
- Baldocchi, D. (2008). 'Breathing' of the terrestrial biosphere: lessons learned from a global network of carbon dioxide flux measurement systems. *Australian Journal of Botany*, 56(1), 1. Retrieved from <http://www.publish.csiro.au/?paper=BT07151> doi: 10.1071/BT07151
- Baldocchi, D., Falge, E., Gu, L., Olson, R., Hollinger, D., Running, S., ... Wofsy, S. (2001, November). FLUXNET: A new tool to study the temporal and spatial variability of ecosystem-scale carbon dioxide, water vapor, and energy flux densities. *Bulletin of the American Meteorological Society*, 82(11), 2415–2434. Retrieved from [http://journals.ametsoc.org/doi/10.1175/1520-0477\(2001\)082%3C2415:FANTTS%3E2.3.CO;2](http://journals.ametsoc.org/doi/10.1175/1520-0477(2001)082%3C2415:FANTTS%3E2.3.CO;2) (ISBN: 0003-0007) doi: 10.1175/1520-0477(2001)082<2415:FANTTS>2.3.CO;2
- Barrett, D. J. (2012). NPP Multi-Biome: VAST Calibration Data, 1965-1998, R1. Retrieved from [http://daac.ornl.gov/cgi-bin/dsviewer.pl?ds\\_id=576](http://daac.ornl.gov/cgi-bin/dsviewer.pl?ds_id=576) (Publisher: ORNL Distributed Active Archive Center) doi: 10.3334/ORNLDAAC/576
- Bolstad, P. V., Davis, K. J., Martin, J., Cook, B. D., & Wang, W. (2004, May). Component and whole-system respiration fluxes in northern deciduous forests. *Tree Physiology*, 24(5), 493–504. Retrieved 2022-06-24, from <https://academic.oup.com/treephys/article-lookup/doi/10.1093/treephys/24.5.493> doi: 10.1093/treephys/24.5.493
- Bridgewater, S., Ibáñez, A., Ratter, J. A., & Furley, P. (2002, November). Vegetation classification and floristics of the savannas and associated wetlands of the Rio Bravo Conservation and Management Area, Belize. *Edinburgh Journal of Botany*, 59(3), 421–442. Retrieved 2022-05-06, from <https://journals.rbgbe.org.uk/ejb/article/view/1265> doi: 10.1017/S0960428602000252
- Burton, A. J., Melillo, J. M., & Frey, S. D. (2008). Adjustment of forest ecosystem root respiration as temperature warms. *Journal of Integrative Plant Biology*, 50(11), 1467–1483. doi: 10.1111/j.1744-7909.2008.00750.x
- Campioli, M., Vicca, S., Luyssaert, S., Bilcke, J., Ceschia, E., Chapin III, F. S., ... Janssens, I. A. (2015, November). Biomass production efficiency controlled by management in temperate and boreal ecosystems. *Nature Geoscience*, 8(11), 843–846. Retrieved 2022-07-18, from <http://www.nature.com/articles/ngeo2553> doi: 10.1038/ngeo2553
- Chen, J., Zhang, H., Liu, Z., Che, M., & Chen, B. (2014, April). Evaluating pa-

- 850 parameter adjustment in the MODIS gross primary production algorithm based  
 851 on eddy covariance tower measurements. *Remote Sensing*, 6(4), 3321–3348.  
 852 Retrieved 2022-07-20, from <http://www.mdpi.com/2072-4292/6/4/3321> doi:  
 853 10.3390/rs6043321
- 854 Chen, J. M., Mo, G., Pisek, J., Liu, J., Deng, F., Ishizawa, M., & Chan, D. (2012,  
 855 March). Effects of foliage clumping on the estimation of global terrestrial gross  
 856 primary productivity. *Global Biogeochemical Cycles*, 26(1), n/a–n/a. Retrieved  
 857 2023-01-29, from <http://doi.wiley.com/10.1029/2010GB003996> doi:  
 858 10.1029/2010GB003996
- 859 Chu, H., Luo, X., Ouyang, Z., Chan, W. S., Dengel, S., Biraud, S. C., ... Zona,  
 860 D. (2021). Representativeness of eddy-covariance flux footprints for ar-  
 861 eas surrounding AmeriFlux sites. *Agricultural and Forest Meteorology*, 301–  
 862 302(February). doi: 10.1016/j.agrformet.2021.108350
- 863 Clark, D. A., Brown, S., Kicklighter, D. W., Chambers, J. Q., Thomlinson, J. R., &  
 864 Ni, J. (2001, April). Measuring net primary production in forests: Concepts  
 865 and field methods. *Ecological Applications*, 11(2), 356–370. Retrieved 2023-  
 866 02-02, from [http://doi.wiley.com/10.1890/1051-0761\(2001\)011\[0356:MNPPIF\]2.0.CO;2](http://doi.wiley.com/10.1890/1051-0761(2001)011[0356:MNPPIF]2.0.CO;2)  
 867 doi: 10.1890/1051-0761(2001)011[0356:MNPPIF]2.0.CO;2
- 868 Collalti, A., & Prentice, I. C. (2019). Is NPP proportional to GPP? War-  
 869 ing's hypothesis 20 years on. *Tree Physiology*, 39(8), 1473–1483. doi:  
 870 10.1093/treephys/tpz034
- 871 Coops, N. C., Jassal, R. S., Leuning, R., Black, A. T., & Morgenstern, K. (2007,  
 872 December). Incorporation of a soil water modifier into MODIS predictions  
 873 of temperate Douglas-fir gross primary productivity: Initial model develop-  
 874 ment. *Agricultural and Forest Meteorology*, 147(3-4), 99–109. Retrieved  
 875 2022-07-20, from <https://linkinghub.elsevier.com/retrieve/pii/S0168192307001700> doi: 10.1016/j.agrformet.2007.07.001
- 876 Cramer, W., Kicklighter, D. W., Bondeau, A., Iii, B. M., Churkina, G., Nemry, B.,  
 877 ... Intercomparison, T. P. O. T. P. (1999, April). Comparing global mod-  
 878 els of terrestrial net primary productivity (NPP): overview and key results.  
 879 *Global Change Biology*, 5(S1), 1–15. Retrieved 2023-02-02, from <https://onlinelibrary.wiley.com/doi/10.1046/j.1365-2486.1999.00009.x> doi:  
 880 10.1046/j.1365-2486.1999.00009.x
- 881 Damesin, C., Ceschia, E., Le Goff, N., Ottorini, J. M., & Dufrêne, E. (2002, Jan-  
 882 uary). Stem and branch respiration of beech: from tree measurements to esti-  
 883 mations at the stand level. *New Phytologist*, 153(1), 159–172. Retrieved 2022-  
 884 06-24, from <http://doi.wiley.com/10.1046/j.0028-646X.2001.00296.x> doi:  
 885 10.1046/j.0028-646X.2001.00296.x
- 886 DeAngelis, D. L., Gardner, R. H., & Shugart, H. H. (2012). NPP Multi-  
 887 Biome: Global IBP Woodlands Data, 1955-1975, R1. Retrieved from  
 888 [http://daac.ornl.gov/cgi-bin/dsviewer.pl?ds\\_id=198](http://daac.ornl.gov/cgi-bin/dsviewer.pl?ds_id=198) (Publisher:  
 889 ORNL Distributed Active Archive Center) doi: 10.3334/ORNLDAAAC/198
- 890 Dennisenko, E. A., Brovkin, V., & Cramer, W. P. (2012). NPP Multi-Biome: PIK  
 891 Data for Northern Eurasia, 1940-1988 (Based on Bazilevich), R1. Retrieved  
 892 from [http://daac.ornl.gov/cgi-bin/dsviewer.pl?ds\\_id=575](http://daac.ornl.gov/cgi-bin/dsviewer.pl?ds_id=575) (Publisher:  
 893 ORNL Distributed Active Archive Center) doi: 10.3334/ORNLDAAAC/575
- 894 Desrochers, A., Landhausser, S. M., & Lieffers, V. J. (2002, July). Coarse and  
 895 fine root respiration in aspen (*Populus tremuloides*). *Tree Physiology*,  
 896 22(10), 725–732. Retrieved 2022-06-27, from <https://academic.oup.com/treephys/article-lookup/doi/10.1093/treephys/22.10.725> doi:  
 897 10.1093/treephys/22.10.725
- 898 Drake, J. E., Stoy, P. C., Jackson, R. B., & DeLucia, E. H. (2008, November). Fine-  
 899 root respiration in a loblolly pine (*Pinus taeda* L.) forest exposed to elevated  
 900 CO<sub>2</sub> and N fertilization. *Plant, Cell & Environment*, 31(11), 1663–1672. Retrieved  
 901 2022-07-13, from <https://onlinelibrary.wiley.com/doi/10.1111/>

- 905 j.1365-3040.2008.01869.x doi: 10.1111/j.1365-3040.2008.01869.x
- 906 Dwyer, J. M., Hobbs, R. J., & Mayfield, M. M. (2014, February). Specific leaf  
907 area responses to environmental gradients through space and time. *Ecology*,  
908 95(2), 399–410. Retrieved 2022-06-03, from <http://doi.wiley.com/10.1890/13-0412.1> doi: 10.1890/13-0412.1
- 910 Díaz, S., Kattge, J., Cornelissen, J. H. C., Wright, I. J., Lavorel, S., Dray, S., ...  
911 Gorné, L. D. (2016, January). The global spectrum of plant form and function.  
912 *Nature*, 529(7585), 167–171. Retrieved from <http://www.nature.com/articles/nature16489> doi: 10.1038/nature16489
- 913 Erb, K.-H., Kastner, T., Plutzar, C., Bais, A. L. S., Carvalhais, N., Fetzel, T., ...  
914 Luyssaert, S. (2018, January). Unexpectedly large impact of forest management  
915 and grazing on global vegetation biomass. *Nature*, 553(7686), 73–76.  
916 Retrieved 2022-07-29, from <http://www.nature.com/articles/nature25138>  
917 doi: 10.1038/nature25138
- 918 Esser, G. (2013). NPP Multi-Biome: Global Osnabruck Data, 1937-1981, R1.  
919 Retrieved from [http://daac.ornl.gov/cgi-bin/dsviewer.pl?ds\\_id=214](http://daac.ornl.gov/cgi-bin/dsviewer.pl?ds_id=214)  
920 (Publisher: ORNL Distributed Active Archive Center) doi: 10.3334/ORNLDAAC/214
- 921 FAO. (2010). *Appendix 4: Alphabetical List of Crops with Botanical Name and Crop Code* (Tech. Rep.). Retrieved 2022-06-17, from [https://www.fao.org/fileadmin/templates/ess/documents/world\\_census\\_of\\_agriculture/appendix4\\_r7.pdf](https://www.fao.org/fileadmin/templates/ess/documents/world_census_of_agriculture/appendix4_r7.pdf)
- 922 Friedl, M., & Sulla-Menashe, D. (2019). MCD12Q1 MODIS/Terra+Aqua Land  
923 Cover Type Yearly L3 Global 500m SIN Grid V006 [Data set].  
924 doi: <https://doi.org/10.5067/MODIS/MCD12Q1.006>
- 925 Friedlingstein, P., O'Sullivan, M., Jones, M. W., Andrew, R. M., Hauck, J., Olsen,  
926 A., ... Zaehle, S. (2020, December). Global Carbon Budget 2020. *Earth System  
927 Science Data*, 12(4), 3269–3340. Retrieved from <https://essd.copernicus.org/articles/12/3269/2020/> doi: 10.5194/essd-12-3269-2020
- 928 Fu, G., Zhang, J., Shen, Z.-X., Shi, P.-L., He, Y.-T., & Zhang, X.-Z. (2017, Au-  
929 gust). Validation of collection of 6 MODIS/Terra and MODIS/Aqua gross  
930 primary production in an alpine meadow of the Northern Tibetan Plateau.  
931 *International Journal of Remote Sensing*, 38(16), 4517–4534. Retrieved  
932 2022-07-14, from <https://www.tandfonline.com/doi/full/10.1080/01431161.2017.1323283>  
933 doi: 10.1080/01431161.2017.1323283
- 934 Funk, J. L., Larson, J. E., Ames, G. M., Butterfield, B. J., Cavender-Bares, J., Firn,  
935 J., ... Wright, J. (2017). Revisiting the Holy Grail: Using plant functional  
936 traits to understand ecological processes. *Biological Reviews*, 92(2), 1156–1173.  
937 (ISBN: 1714744795) doi: 10.1111/brv.12275
- 938 Gan, R., Zhang, L., Yang, Y., Wang, E., Woodgate, W., Zhang, Y., ... Yu, Q. (2021,  
939 October). Estimating ecosystem maximum light use efficiency based on the  
940 water use efficiency principle. *Environmental Research Letters*, 16(10), 104032.  
941 Retrieved 2022-07-20, from <https://iopscience.iop.org/article/10.1088/1748-9326/ac263b> doi: 10.1088/1748-9326/ac263b
- 942 Garbulsky, M. F., Peñuelas, J., Papale, D., Ardö, J., Goulden, M. L., Kiely, G.,  
943 ... Filella, I. (2010, March). Patterns and controls of the variability of  
944 radiation use efficiency and primary productivity across terrestrial ecosys-  
945 tems. *Global Ecology and Biogeography*, 19(2), 253–267. Retrieved from  
946 <http://doi.wiley.com/10.1111/j.1466-8238.2009.00504.x> doi:  
947 10.1111/j.1466-8238.2009.00504.x
- 948 Gelaro, R., McCarty, W., Suárez, M. J., Todling, R., Molod, A., Takacs, L., ...  
949 Zhao, B. (2017, July). The Modern-Era Retrospective Analysis for Re-  
950 search and Applications, Version 2 (MERRA-2). *Journal of Climate*, 30(14),  
951 5419–5454. Retrieved from <http://journals.ametsoc.org/doi/10.1175/JCLI-D-16-0758.1>  
952 doi: 10.1175/JCLI-D-16-0758.1
- 953
- 954
- 955
- 956
- 957
- 958
- 959

- 960 Gong, H., & Gao, J. (2019, October). Soil and climatic drivers of plant SLA (specific leaf area). *Global Ecology and Conservation*, 20, e00696. Retrieved 2022-07-20, from <https://linkinghub.elsevier.com/retrieve/pii/S2351989419302665> doi: 10.1016/j.gecco.2019.e00696
- 961  
962  
963  
964  
965  
966  
967  
968  
969  
970  
971  
972  
973  
974  
975  
976  
977  
978  
979  
980  
981  
982  
983  
984  
985  
986  
987  
988  
989  
990  
991  
992  
993  
994  
995  
996  
997  
998  
999  
1000  
1001  
1002  
1003  
1004  
1005  
1006  
1007  
1008  
1009  
1010  
1011  
1012  
1013  
Gower, S. T., Krankina, O. N., Olson, R. J., Apps, M. J., Linder, S., & Wang, C. (2012). NPP Boreal Forest: Consistent Worldwide Site Estimates, 1965-1995, R1. Retrieved from [http://daac.ornl.gov/cgi-bin/dsviewer.pl?ds\\_id=611](http://daac.ornl.gov/cgi-bin/dsviewer.pl?ds_id=611) (Publisher: ORNL Distributed Active Archive Center) doi: 10.3334/ORNLDAAAC/611
- Gower, S. T., & Richards, J. H. (1990, December). Larches: Deciduous Conifers in an Evergreen World. *BioScience*, 40(11), 818–826. Retrieved 2022-12-19, from <https://academic.oup.com/bioscience/article-lookup/doi/10.2307/1311484> doi: 10.2307/1311484
- Guan, X., Chen, J. M., Shen, H., Xie, X., & Tan, J. (2022, February). Comparison of big-leaf and two-leaf light use efficiency models for GPP simulation after considering a radiation scalar. *Agricultural and Forest Meteorology*, 313, 108761. Retrieved 2022-07-20, from <https://linkinghub.elsevier.com/retrieve/pii/S0168192321004470> doi: 10.1016/j.agrformet.2021.108761
- Heinsch, F. A., Zhao, M., Running, S. W., Kimball, J. S., Nemani, R. R., Davis, K. J., ... Flanagan, L. B. (2006, July). Evaluation of remote sensing based terrestrial productivity from MODIS using regional tower eddy flux network observations. *IEEE Transactions on Geoscience and Remote Sensing*, 44(7), 1908–1923. Retrieved from <http://ieeexplore.ieee.org/document/1645290/> doi: 10.1109/TGRS.2005.853936
- Herman, J., & Usher, W. (2017, January). SALib: An open-source Python library for Sensitivity Analysis. *The Journal of Open Source Software*, 2(9), 97. Retrieved 2022-06-18, from <http://joss.theoj.org/papers/10.21105/joss.00097> doi: 10.21105/joss.00097
- Huang, X., Ma, M., Wang, X., Tang, X., & Yang, H. (2018, December). The uncertainty analysis of the MODIS GPP product in global maize crop lands. *Frontiers of Earth Science*, 12(4), 739–749. Retrieved 2023-01-25, from <http://link.springer.com/10.1007/s11707-018-0716-x> doi: 10.1007/s11707-018-0716-x
- Huntzinger, D. N., Schwalm, C., Michalak, A. M., Schaefer, K., King, A. W., Wei, Y., ... Zhu, Q. (2013, December). The North American Carbon Program Multi-Scale Synthesis and Terrestrial Model Intercomparison Project – Part 1: Overview and experimental design. *Geoscientific Model Development*, 6(6), 2121–2133. Retrieved 2014-01-23, from <http://www.geosci-model-dev.net/6/2121/2013/> doi: 10.5194/gmd-6-2121-2013
- Högberg, P., Nordgren, A., Buchmann, N., Taylor, A. F. S., Ekblad, A., Högberg, M. N., ... Read, D. J. (2001, June). Large-scale forest girdling shows that current photosynthesis drives soil respiration. *Nature*, 411(6839), 789–792. Retrieved from <http://www.nature.com/articles/35081058> doi: 10.1038/35081058
- Ito, A. (2011, October). A historical meta-analysis of global terrestrial net primary productivity: are estimates converging?: A HISTORICAL META-ANALYSIS OF GLOBAL LAND NPP. *Global Change Biology*, 17(10), 3161–3175. Retrieved 2023-02-02, from <https://onlinelibrary.wiley.com/doi/10.1111/j.1365-2486.2011.02450.x> doi: 10.1111/j.1365-2486.2011.02450.x
- Iversen, C. M., McCormack, M. L., Powell, A. S., Blackwood, C. B., Freschet, G. T., Kattge, J., ... Vialle, C. (2017, July). A global Fine-Root Ecology Database to address below-ground challenges in plant ecology. *New Phytologist*, 215(1), 15–26. Retrieved 2022-05-17, from <https://onlinelibrary.wiley.com/doi/10.1111/nph.14486> doi: 10.1111/nph.14486

- 1014 Iwanaga, T., Usher, W., & Herman, J. (2022). Toward SALib 2.0: Advanc-  
 1015 ing the accessibility and interpretability of global sensitivity analyses.  
 1016 *Socio-Environmental Systems Modeling*, 4. doi: <https://doi.org/10.18174/sesmo.18155>
- 1017 Ji, Y., Zhou, G., Luo, T., Dan, Y., Zhou, L., & Lv, X. (2020, December). Variation  
 1018 of net primary productivity and its drivers in China's forests during 2000–  
 1019 2018. *Forest Ecosystems*, 7(1), 15. Retrieved 2022-08-03, from <https://forestecosyst.springeropen.com/articles/10.1186/s40663-020-00229-0>  
 1020 doi: 10.1186/s40663-020-00229-0
- 1021 Joiner, J., Yoshida, Y., Zhang, Y., Duveiller, G., Jung, M., Lyapustin, A., ... Tucker,  
 1022 C. (2018, August). Estimation of Terrestrial Global Gross Primary Pro-  
 1023 duction (GPP) with Satellite Data-Driven Models and Eddy Covariance  
 1024 Flux Data. *Remote Sensing*, 10(9), 1346. Retrieved 2023-01-29, from  
 1025 <http://www.mdpi.com/2072-4292/10/9/1346> doi: 10.3390/rs10091346
- 1026 Jones, L. A., Kimball, J. S., Reichle, R. H., Madani, N., Glassy, J., Ardizzone, J. V.,  
 1027 ... Scott, R. L. (2017). The SMAP Level 4 Carbon Product for Monitoring  
 1028 Ecosystem Land-Atmosphere CO<sub>2</sub> Exchange. *IEEE Transactions on Geo-  
 1029 science and Remote Sensing*, 55(11), 6517–6532. (ISBN: 9781509033324) doi:  
 1030 10.1109/TGRS.2017.2729343
- 1031 Jones, M. O., Running, S. W., Kimball, J. S., Robinson, N. P., & Allred, B. W.  
 1032 (2020, December). Terrestrial primary productivity indicators for inclusion in  
 1033 the National Climate Indicators System. *Climatic Change*, 163(4), 1855–1868.  
 1034 Retrieved from <http://link.springer.com/10.1007/s10584-018-2155-9>  
 1035 doi: 10.1007/s10584-018-2155-9
- 1036 Jung, M., Schwalm, C., Migliavacca, M., Walther, S., Camps-Valls, G., Koirala, S.,  
 1037 ... Reichstein, M. (2020). Scaling carbon fluxes from eddy covariance sites to  
 1038 globe: Synthesis and evaluation of the FLUXCOM approach. *Biogeosciences*,  
 1039 17(5), 1343–1365. doi: 10.5194/bg-17-1343-2020
- 1040 Justice, C., Townshend, J. R. G., Vermote, E. F., Masuoka, E., Wolfe, R., Saleous,  
 1041 N., ... Morisette, J. T. (2002, November). An overview of MODIS Land data  
 1042 processing and product status. *Remote Sensing of Environment*, 83(1-2), 3–15.  
 1043 Retrieved 2022-07-04, from <https://linkinghub.elsevier.com/retrieve/pii/S0034425702000846> doi: 10.1016/S0034-4257(02)00084-6
- 1044 Kanamitsu, M., Ebisuzaki, W., Woollen, J., Yang, S.-K., Hnilo, J. J., Fiorino, M.,  
 1045 ... Potter, G. L. (2002, November). NCEP–DOE AMIP-II Reanalysis (R-2).  
 1046 *Bulletin of the American Meteorological Society*, 83(11), 1631–1644. Re-  
 1047 tried 2023-02-14, from <https://journals.ametsoc.org/doi/10.1175/BAMS-83-11-1631> doi: 10.1175/BAMS-83-11-1631
- 1048 Kattge, J., Bönisch, G., Díaz, S., Lavorel, S., Prentice, I. C., Leadley, P., ...  
 1049 (2020). TRY plant trait database – enhanced coverage and open access. *Global  
 1050 Change Biology*, 26(1), 119–188. doi: 10.1111/gcb.14904
- 1051 Kicklighter, D. W. (2012). NPP Multi-Biome: TEM Calibration Data, 1992, R1.  
 1052 Retrieved from [http://daac.ornl.gov/cgi-bin/dsviewer.pl?ds\\_id=471](http://daac.ornl.gov/cgi-bin/dsviewer.pl?ds_id=471)  
 1053 (Publisher: ORNL Distributed Active Archive Center) doi: 10.3334/  
 1054 ORNLDAAC/471
- 1055 Kicklighter, D. W., Bruno, M., DZönges, S., Esser, G., Heimann, M., Helfrich, J., ...  
 1056 Würth, G. (1999, January). A first-order analysis of the potential role of CO<sub>2</sub>  
 1057 fertilization to affect the global carbon budget: A comparison of four terres-  
 1058 trial biosphere models. *Tellus B: Chemical and Physical Meteorology*, 51(2),  
 1059 343–366. Retrieved from <https://www.tandfonline.com/doi/full/10.3402/tellusb.v51i2.16303> doi: 10.3402/tellusb.v51i2.16303
- 1060 Kloepfel, B. D., Treichel, I. W., Kharuk, S., & Gower, S. T. (1998, April). Fo-  
 1061 liar carbon isotope discrimination in Larix species and sympatric evergreen  
 1062 conifers: a global comparison. *Oecologia*, 114(2), 153–159. Retrieved 2022-  
 1063 12-19, from <http://link.springer.com/10.1007/s004420050431> doi:  
 1064

- 1069 10.1007/s004420050431  
 1070 Kushida, K., Isaev, A. P., Maximov, T. C., Takao, G., & Fukuda, M. (2007,  
 1071 April). Remote sensing of upper canopy leaf area index and forest floor  
 1072 vegetation cover as indicators of net primary productivity in a Siberian  
 1073 larch forest. *Journal of Geophysical Research*, 112(G2), G02003. Retrieved  
 1074 2022-07-21, from <http://doi.wiley.com/10.1029/2006JG000269> doi:  
 1075 10.1029/2006JG000269
- 1076 Lavigne, M. B., Franklin, S. E., & Hunt, E. R. (1996, August). Estimating stem  
 1077 maintenance respiration rates of dissimilar balsam fir stands. *Tree Physiology*,  
 1078 16(8), 687–695. Retrieved 2022-06-24, from <https://academic.oup.com/treephys/article-lookup/doi/10.1093/treephys/16.8.687> doi:  
 1080 10.1093/treephys/16.8.687
- 1081 Le Quéré, C., Barbero, L., Hauck, J., Andrew, R. M., Canadell, J. G., Sitch, S., &  
 1082 Korsbakken, J. I. (2018). Global Carbon Budget 2018. *Earth System Science  
 1083 Data*, 10, 2141–2194.
- 1084 Liu, Y., Holtzman, N. M., & Konings, A. G. (2021, May). Global ecosystem-  
 1085 scale plant hydraulic traits retrieved using model-data fusion. *Hydrol-  
 1086 ogy and Earth System Sciences*, 25(5), 2399–2417. Retrieved 2022-09-26,  
 1087 from <https://hess.copernicus.org/articles/25/2399/2021/> doi:  
 1088 10.5194/hess-25-2399-2021
- 1089 Liu, Z., Zhao, M., Zhang, H., Ren, T., Liu, C., & He, N. (2022, November).  
 1090 Divergent response and adaptation of specific leaf area to environmen-  
 1091 tal change at different spatio-temporal scales jointly improve plant sur-  
 1092 vival. *Global Change Biology*, gcb.16518. Retrieved 2022-12-18, from  
 1093 <https://onlinelibrary.wiley.com/doi/10.1111/gcb.16518> doi:  
 1094 10.1111/gcb.16518
- 1095 Luo, Z., Xiao, L., Wang, G., Chang, J., Chen, Y., Guo, X., ... Jia, S. (2021,  
 1096 May). *Depth distribution of belowground net primary production across  
 1097 global biomes* (preprint). In Review. Retrieved 2022-07-28, from  
 1098 <https://www.researchsquare.com/article/rs-65178/v3> doi: 10.21203/  
 1099 rs.3.rs-65178/v3
- 1100 Lynch, D. J., Matamala, R., Iversen, C. M., Norby, R. J., & Gonzalez-Meler, M. A.  
 1101 (2013, July). Stored carbon partly fuels fine-root respiration but is not used  
 1102 for production of new fine roots. *New Phytologist*, 199(2), 420–430. Retrieved  
 1103 2022-07-15, from <https://onlinelibrary.wiley.com/doi/10.1111/nph.12290> doi: 10.1111/nph.12290
- 1104 Madani, N., Kimball, J. S., Ballantyne, A. P., Affleck, D. L. R., van Bodegom,  
 1105 P. M., Reich, P. B., ... Running, S. W. (2018, February). Future global pro-  
 1106 ductivity will be affected by plant trait response to climate. *Scientific Reports*,  
 1107 8(1), 2870. Retrieved 2023-01-29, from <https://www.nature.com/articles/s41598-018-21172-9> doi: 10.1038/s41598-018-21172-9
- 1108 Madani, N., Kimball, J. S., & Running, S. W. (2017). Improving global gross pri-  
 1109 mary productivity estimates by computing optimum light use efficiencies using  
 1110 flux tower data. *Journal of Geophysical Research: Biogeosciences*, 122(11),  
 1111 2939–2951. doi: 10.1002/2017JG004142
- 1112 Madani, N., Parazoo, N. C., Kimball, J. S., Ballantyne, A. P., Reichle, R. H.,  
 1113 Maneta, M., ... Tagesson, T. (2020, December). Recent Amplified Global  
 1114 Gross Primary Productivity Due to Temperature Increase Is Offset by Reduced  
 1115 Productivity Due to Water Constraints. *AGU Advances*, 1(4). Retrieved 2023-  
 1116 01-29, from <https://onlinelibrary.wiley.com/doi/10.1029/2020AV000180> doi: 10.1029/2020AV000180
- 1117 Malhi, Y. (2012, January). The productivity, metabolism and carbon cy-  
 1118 cle of tropical forest vegetation: Carbon cycle of tropical forests. *Jour-  
 1119 nal of Ecology*, 100(1), 65–75. Retrieved 2023-02-14, from <https://onlinelibrary.wiley.com/doi/10.1111/j.1365-2745.2011.01916.x> doi:

- 10.1111/j.1365-2745.2011.01916.x
- Meek, D. W., Hatfield, J. L., Howell, T. A., Idso, S. B., & Reginato, R. J. (1984, November). A Generalized Relationship between Photosynthetically Active Radiation and Solar Radiation. *Agronomy Journal*, 76(6), 939–945. Retrieved 2022-09-19, from <https://onlinelibrary.wiley.com/doi/10.2134/agronj1984.00021962007600060018x> doi: 10.2134/agronj1984.00021962007600060018x
- Murphy, R. E., Barnes, W. L., Lyapustin, A. I., Privette, J., Welsch, C., DeLuccia, F., ... Kealy, P. S. M. (2001). Using VIIRS to provide data continuity with MODIS. In *IGARSS 2001. Scanning the Present and Resolving the Future. Proceedings. IEEE 2001 International Geoscience and Remote Sensing Symposium (Cat. No.01CH37217)* (Vol. 3, pp. 1212–1214). Sydney, NSW, Australia: IEEE. Retrieved 2022-07-07, from <http://ieeexplore.ieee.org/document/976795/> doi: 10.1109/IGARSS.2001.976795
- Myneni, R. B. (2018). *VIIRS Leaf Area Index (LAI) and Fraction of Photosynthetically Active Radiation Absorbed by Vegetation (FPAR) User Guide* (Tech. Rep.). Department of Earth and Environment, Boston University. Retrieved 2022-07-22, from [https://lpdaac.usgs.gov/documents/126/VNP15\\_User\\_Guide.pdf](https://lpdaac.usgs.gov/documents/126/VNP15_User_Guide.pdf)
- Myneni, R. B., Knyazikhin, Y., & Park, T. (2015). *MODIS/Terra+Aqua Leaf Area Index/FPAR 8-day L4 Global 500m SIN Grid V006 [Data set]*. Retrieved 2021-07-02, from <https://doi.org/10.5067/MODIS/MOD15A2H.061> doi: <https://doi.org/10.5067/MODIS/MOD15A2H.061>
- Olson, R. J., Scurlock, J. M. O., Prince, S. D., Zheng, D. L., & Johnson, K. R. (2013). NPP Multi-Biome: Global Primary Production Data Initiative Products, R2. Retrieved from [http://daac.ornl.gov/cgi-bin/dsviewer.pl?ds\\_id=617](http://daac.ornl.gov/cgi-bin/dsviewer.pl?ds_id=617) (Publisher: ORNL Distributed Active Archive Center) doi: 10.3334/ORNLDAAAC/617
- Olson, R. J., Scurlock, J. M. O., Walker, T. R., Hook, L. A., Curtis, C. N., & Cook, R. B. (2017). NPP Multi-Biome: Summary Data from Intensive Studies at 125 Sites, 1936-2006. Retrieved from [http://daac.ornl.gov/cgi-bin/dsviewer.pl?ds\\_id=1352](http://daac.ornl.gov/cgi-bin/dsviewer.pl?ds_id=1352) (Publisher: ORNL Distributed Active Archive Center) doi: 10.3334/ORNLDAAAC/1352
- Piao, S., Sitch, S., Ciais, P., Friedlingstein, P., Peylin, P., Wang, X., ... Zeng, N. (2013, July). Evaluation of terrestrial carbon cycle models for their response to climate variability and to CO<sub>2</sub> trends. *Global Change Biology*, 19(7), 2117–2132. Retrieved 2023-01-29, from <https://onlinelibrary.wiley.com/doi/10.1111/gcb.12187> doi: 10.1111/gcb.12187
- Poorter, H., Niinemets, ., Poorter, L., Wright, I. J., & Villar, R. (2009, May). Causes and consequences of variation in leaf mass per area (LMA): a meta-analysis. *New Phytologist*, 182(3), 565–588. Retrieved 2022-06-21, from <https://onlinelibrary.wiley.com/doi/10.1111/j.1469-8137.2009.02830.x> doi: 10.1111/j.1469-8137.2009.02830.x
- Propastin, P., Ibrom, A., Knohl, A., & Erasmi, S. (2012, June). Effects of canopy photosynthesis saturation on the estimation of gross primary productivity from MODIS data in a tropical forest. *Remote Sensing of Environment*, 121, 252–260. Retrieved 2022-07-04, from <https://linkinghub.elsevier.com/retrieve/pii/S0034425712000892> doi: 10.1016/j.rse.2012.02.005
- Reich, P. B., Ellsworth, D. S., & Walters, M. B. (1998, December). Leaf structure (specific leaf area) modulates photosynthesis-nitrogen relations: evidence from within and across species and functional groups: SLA regulates photosynthetic nitrogen use. *Functional Ecology*, 12(6), 948–958. Retrieved 2022-06-21, from <http://doi.wiley.com/10.1046/j.1365-2435.1998.00274.x> doi: 10.1046/j.1365-2435.1998.00274.x

- 1178 Running, S. W., Nemani, R. R., Heinsch, F. A., Zhao, M., Reeves, M., & Hashimoto,  
 1179 H. (2004). A continuous satellite-derived measure of global terrestrial primary  
 1180 production. *BioScience*, 54(6), 547. Retrieved from <https://academic.oup.com/bioscience/article/54/6/547-560/294347> (arXiv: 1011.1669v3  
 1181 ISBN: 0006-3568) doi: 10.1641/0006-3568(2004)054[0547:acsmog]2.0.co;2  
 1182
- 1183 Running, S. W., & Zhao, M. (2021). *User's Guide Daily GPP and Annual NPP  
 1184 (MOD17A2H/A3H) and Year-end Gap- Filled (MOD17A2HGF/A3HGF)  
 1185 Products NASA Earth Observing System MODIS Land Algorithm (For  
 1186 Collection 6.1)* (Tech. Rep. No. Version 1.1). Retrieved 2022-06-16, from  
 1187 [https://lpdaac.usgs.gov/documents/926/MOD15\\_User\\_Guide\\_V61.pdf](https://lpdaac.usgs.gov/documents/926/MOD15_User_Guide_V61.pdf)
- 1188 Ryan, M. G., Gower, S. T., Hubbard, R. M., Waring, R. H., Gholz, H. L., Cropper,  
 1189 W. P., & Running, S. W. (1995, February). Woody tissue maintenance res-  
 1190piration of four conifers in contrasting climates. *Oecologia*, 101(2), 133–140.  
 1191 Retrieved 2022-06-27, from <http://link.springer.com/10.1007/BF00317276>  
 1192 doi: 10.1007/BF00317276
- 1193 Ryu, Y., Berry, J. A., & Baldocchi, D. D. (2019). What is global photosynthe-  
 1194 sis? History, uncertainties and opportunities. *Remote Sensing of Environ-  
 1195 ment*, 223(January), 95–114. Retrieved from <https://doi.org/10.1016/j.rse.2019.01.016> (Publisher: Elsevier) doi: 10.1016/j.rse.2019.01.016
- 1196 Salvatier, J., Wiecki, T. V., & Fonnesbeck, C. (2016, April). Probabilistic program-  
 1197 ming in Python using PyMC3. *PeerJ Computer Science*, 2, e55. Retrieved  
 1198 2022-06-27, from <https://peerj.com/articles/cs-55> doi: 10.7717/peerj-cs  
 1199 .55
- 1200 Scurlock, J. M. O., Johnson, K. R., & Olson, R. J. (2003). NPP Grassland: NPP  
 1201 Estimates from Biomass Dynamics for 31 Sites, 1948-1994, R1. Retrieved  
 1202 from [http://daac.ornl.gov/cgi-bin/dsviewer.pl?ds\\_id=654](http://daac.ornl.gov/cgi-bin/dsviewer.pl?ds_id=654) (Publisher:  
 1203 ORNL Distributed Active Archive Center) doi: 10.3334/ORNLDaac/654
- 1204 Scurlock, J. M. O., & Olson, R. J. (2012). NPP Multi-Biome: Grassland, Boreal  
 1205 Forest, and Tropical Forest Sites, 1939-1996, R1. Retrieved from [http://daac.ornl.gov/cgi-bin/dsviewer.pl?ds\\_id=653](http://daac.ornl.gov/cgi-bin/dsviewer.pl?ds_id=653) (Publisher: ORNL Distributed  
 1206 Active Archive Center) doi: 10.3334/ORNLDaac/653
- 1207 Sitch, S., Friedlingstein, P., Gruber, N., Jones, S. D., Murray-Tortarolo, G.,  
 1208 Ahlström, A., ... Myneni, R. (2015). Recent trends and drivers of regional  
 1209 sources and sinks of carbon dioxide. *Biogeosciences*, 12(3), 653–679. doi:  
 1210 10.5194/bg-12-653-2015
- 1211 Sjöström, M., Zhao, M., Archibald, S., Arneth, A., Cappelaere, B., Falk, U., ... Ardö,  
 1212 J. (2013, April). Evaluation of MODIS gross primary productivity for Africa  
 1213 using eddy covariance data. *Remote Sensing of Environment*, 131, 275–286.  
 1214 Retrieved 2022-07-04, from <https://linkinghub.elsevier.com/retrieve/pii/S0034425712004890> doi: 10.1016/j.rse.2012.12.023
- 1215 Skakun, S., Justice, C. O., Vermote, E., & Roger, J.-C. (2018, February).  
 1216 Transitioning from MODIS to VIIRS: an analysis of inter-consistency of  
 1217 NDVI data sets for agricultural monitoring. *International Journal of  
 1218 Remote Sensing*, 39(4), 971–992. Retrieved 2022-07-07, from <https://www.tandfonline.com/doi/full/10.1080/01431161.2017.1395970> doi:  
 1219 10.1080/01431161.2017.1395970
- 1220 Sobol', I. M. (2001, February). Global sensitivity indices for nonlinear math-  
 1221 ematical models and their Monte Carlo estimates. *Mathematics and  
 1222 Computers in Simulation*, 55(1-3), 271–280. Retrieved 2022-06-18, from  
 1223 <https://linkinghub.elsevier.com/retrieve/pii/S0378475400002706>  
 1224 doi: 10.1016/S0378-4754(00)00270-6
- 1225 Stockfors, J., & Linder, S. (1998, March). Effect of nitrogen on the seasonal  
 1226 course of growth and maintenance respiration in stems of Norway spruce  
 1227 trees. *Tree Physiology*, 18(3), 155–166. Retrieved 2022-06-24, from  
 1228 <https://academic.oup.com/treephys/article-lookup/doi/10.1093/>

- treephys/18.3.155 doi: 10.1093/treephys/18.3.155

Sulla-Menashe, D., Gray, J. M., Abercrombie, S. P., & Friedl, M. A. (2019, March). Hierarchical mapping of annual global land cover 2001 to present: The MODIS Collection 6 Land Cover product. *Remote Sensing of Environment*, 222, 183–194. Retrieved from <https://linkinghub.elsevier.com/retrieve/pii/S0034425718305686> doi: 10.1016/j.rse.2018.12.013

Tang, R., Shao, K., Li, Z. L., Wu, H., Tang, B.-H., Zhou, G., & Zhang, L. (2015). Multiscale Validation of the 8-day MOD16 Evapotranspiration Product Using Flux Data Collected in China. *IEEE Journal of Selected Topics in Applied Earth Observations and Remote Sensing*, 8(4), 1478–1486. doi: 10.1109/JSTARS.2015.2420105

Tang, X., Fan, S., Du, M., Zhang, W., Gao, S., Liu, S., ... Yang, W. (2020, May). Spatial and temporal patterns of global soil heterotrophic respiration in terrestrial ecosystems. *Earth System Science Data*, 12(2), 1037–1051. Retrieved from <https://essd.copernicus.org/articles/12/1037/2020/> doi: 10.5194/essd-12-1037-2020

Ter Braak, C. J. F., & Vrugt, J. A. (2008). Differential Evolution Markov Chain with snooker updater and fewer chains. *Statistics and Computing*, 18(4), 435–446. doi: 10.1007/s11222-008-9104-9

Tjoelker, M. G., Oleksyn, J., & Reich, P. B. (2001, February). Modelling respiration of vegetation: Evidence for a general temperature-dependent Q10. *Global Change Biology*, 7(2), 223–230. Retrieved from <http://doi.wiley.com/10.1046/j.1365-2486.2001.00397.x> doi: 10.1046/j.1365-2486.2001.00397.x

Verheijen, L. M., Aerts, R., Brovkin, V., Cavender-Bares, J., Cornelissen, J. H. C., Kattge, J., & van Bodegom, P. M. (2015, August). Inclusion of ecologically based trait variation in plant functional types reduces the projected land carbon sink in an earth system model. *Global Change Biology*, 21(8), 3074–3086. Retrieved 2022-07-20, from <https://onlinelibrary.wiley.com/doi/10.1111/gcb.12871> doi: 10.1111/gcb.12871

Vrugt, J. A., Ter Braak, C. J. F., Diks, C. G. H., Robinson, B. A., Hyman, J. M., & Higdon, D. (2009). Accelerating Markov chain Monte Carlo simulation by differential evolution with self-adaptive randomized subspace sampling. *International Journal of Nonlinear Sciences and Numerical Simulation*, 10(3), 273–290. doi: 10.1515/IJNSNS.2009.10.3.273

Wang, J., & Ogawa, S. (2017, February). Analysis of dynamic changes in land use based on landscape metrics in Nagasaki, Japan. *Journal of Applied Remote Sensing*, 11(1), 016022. Retrieved from <http://remotesensing.spiedigitallibrary.org/article.aspx?doi=10.1117/1.JRS.11.016022> doi: 10.1117/1.JRS.11.016022

Welp, L. R., Keeling, R. F., Meijer, H. A. J., Bollenbacher, A. F., Piper, S. C., Yoshimura, K., ... Wahlen, M. (2011, September). Interannual variability in the oxygen isotopes of atmospheric CO<sub>2</sub> driven by El Niño. *Nature*, 477(7366), 579–582. Retrieved 2023-01-29, from <http://www.nature.com/articles/nature10421> doi: 10.1038/nature10421

White, M. A., Thornton, P. E., Running, S. W., & Nemani, R. R. (2000, January). Parameterization and sensitivity analysis of the BIOME–BGC terrestrial ecosystem model: Net primary production controls. *Earth Interactions*, 4(3), 1–85. Retrieved 2022-06-01, from [http://journals.ametsoc.org/doi/10.1175/1087-3562\(2000\)004<0003:PASAOT>2.0.CO;2](http://journals.ametsoc.org/doi/10.1175/1087-3562(2000)004<0003:PASAOT>2.0.CO;2) doi: 10.1175/1087-3562(2000)004<0003:PASAOT>2.0.CO;2

White, R., & Engelen, G. (2000, September). High-resolution integrated modelling of the spatial dynamics of urban and regional systems. *Computers, Environment and Urban Systems*, 24(5), 383–400. Retrieved from <http://linkinghub.elsevier.com/retrieve/pii/S0198971500000120> doi: 10.1016/S0198-9715(00)00012-0

- 1288 Wright, I. J., Reich, P. B., Westoby, M., Ackerly, D. D., Baruch, Z., Bongers, F.,  
 1289 ... Villar, R. (2004, April). The worldwide leaf economics spectrum. *Nature*,  
 1290 428(6985), 821–827. Retrieved from <http://www.nature.com/articles/nature02403> doi: 10.1038/nature02403
- 1291 Wright, I. J., & Westoby, M. (2001, March). Understanding seedling growth re-  
 1292 lationships through specific leaf area and leaf nitrogen concentration: gen-  
 1293 eralisations across growth forms and growth irradiance. *Oecologia*, 127(1),  
 1294 21–29. Retrieved 2022-07-20, from <http://link.springer.com/10.1007/s004420000554> doi: 10.1007/s004420000554
- 1295 Xiong, X., Angal, A., Chang, T., Chiang, K., Lei, N., Li, Y., ... Wu, A. (2020,  
 1296 September). MODIS and VIIRS calibration and characterization in support  
 1297 of producing long-term high-quality data products. *Remote Sensing*, 12(19),  
 1298 3167. Retrieved 2022-07-07, from <https://www.mdpi.com/2072-4292/12/19/3167> doi: 10.3390/rs12193167
- 1299 Xu, B., Park, T., Yan, K., Chen, C., Zeng, Y., Song, W., ... Myneni, R. B. (2018).  
 1300 Analysis of global LAI/FPAR products from VIIRS and MODIS sensors for  
 1301 spatio-temporal consistency and uncertainty from 2012–2016. *Forests*, 9(2),  
 1302 1–21. doi: 10.3390/f9020073
- 1303 Yan, K., Pu, J., Park, T., Xu, B., Zeng, Y., Yan, G., ... Myneni, R. B. (2021, July).  
 1304 Performance stability of the MODIS and VIIRS LAI algorithms inferred from  
 1305 analysis of long time series of products. *Remote Sensing of Environment*, 260,  
 1306 112438. Retrieved from <https://linkinghub.elsevier.com/retrieve/pii/S0034425721001565> doi: 10.1016/j.rse.2021.112438
- 1307 Yang, R., Wang, J., Zeng, N., Sitch, S., Tang, W., McGrath, M. J., ... Han, P.  
 1308 (2022). Divergent historical GPP trends among state-of-the-art multi-model  
 1309 simulations and satellite-based products. *Earth System Dynamics*(13), 833–  
 1310 849. doi: <https://doi.org/10.5194/esd-13-833-2022>
- 1311 Yuan, W., Cai, W., Liu, S., Dong, W., Chen, J., Arain, M. A., ... Xia, J. (2014,  
 1312 November). Vegetation-specific model parameters are not required for es-  
 1313 timating gross primary production. *Ecological Modelling*, 292, 1–10. Re-  
 1314 tried 2022-07-20, from <https://linkinghub.elsevier.com/retrieve/pii/S0304380014003962> doi: 10.1016/j.ecolmodel.2014.08.017
- 1315 Zaks, D. P. M., Ramankutty, N., Barford, C. C., & Foley, J. A. (2007, Septem-  
 1316 ber). From Miami to Madison: Investigating the relationship between climate  
 1317 and terrestrial net primary production. *Global Biogeochemical Cycles*, 21(3),  
 1318 n/a–n/a. Retrieved 2022-07-18, from <http://doi.wiley.com/10.1029/2006GB002705> doi: 10.1029/2006GB002705
- 1319 Zha, T., Kellomäki, S., Wang, K.-Y., Ryypö, A., & Niinistö, S. (2004, October).  
 1320 Seasonal and annual stem respiration of scots pine trees under boreal con-  
 1321 ditions. *Annals of Botany*, 94(6), 889–896. Retrieved 2022-06-09, from  
 1322 <https://academic.oup.com/aob/article-lookup/doi/10.1093/aob/mch218>  
 1323 doi: 10.1093/aob/mch218
- 1324 Zhang, K., Zhu, G., Ma, J., Yang, Y., Shang, S., & Gu, C. (2019). Parameter  
 1325 analysis and estimates for the MODIS evapotranspiration algorithm and  
 1326 multiscale verification. *Water Resources Research*, 55(3), 2211–2231. doi:  
 1327 10.1029/2018WR023485
- 1328 Zhang, Y., Song, C., Band, L. E., Sun, G., & Li, J. (2017, March). Reanaly-  
 1329 sis of global terrestrial vegetation trends from MODIS products: Browning  
 1330 or greening? *Remote Sensing of Environment*, 191, 145–155. Retrieved  
 1331 2023-02-10, from <https://linkinghub.elsevier.com/retrieve/pii/S0034425716304977> doi: 10.1016/j.rse.2016.12.018
- 1332 Zhang, Y., Xiao, X., Wu, X., Zhou, S., Zhang, G., Qin, Y., & Dong, J. (2017, Octo-  
 1333 ber). A global moderate resolution dataset of gross primary production of veg-  
 1334 etation for 2000–2016. *Scientific Data*, 4(1), 170165. Retrieved 2023-01-29,  
 1335 from <https://www.nature.com/articles/sdata2017165> doi: 10.1038/sdata

- .2017.165  
1343  
1344 Zhang, Y., Yu, Q., Jiang, J., & Tang, Y. (2008, April). Calibration of  
1345 Terra/MODIS gross primary production over an irrigated cropland on the  
1346 North China Plain and an alpine meadow on the Tibetan Plateau. *Global  
1347 Change Biology*, 14(4), 757–767. Retrieved 2023-01-12, from <https://onlinelibrary.wiley.com/doi/10.1111/j.1365-2486.2008.01538.x> doi:  
1348 10.1111/j.1365-2486.2008.01538.x  
1349  
1350 Zhao, M., Heinsch, F. A., Nemani, R. R., & Running, S. W. (2005). Improvements  
1351 of the MODIS terrestrial gross and net primary production global data set. *Re-  
1352 mote Sensing of Environment*, 95, 164–176. doi: 10.1016/j.rse.2004.12.011  
1353 Zhao, M., & Running, S. W. (2010). Drought-induced reduction in global terrestrial  
1354 net Primary production from 2000 through 2009. *Science*, 329, 940–943.  
1355 Zhao, M., Running, S. W., & Nemani, R. R. (2006). Sensitivity of Moderate Res-  
1356 olution Imaging Spectroradiometer (MODIS) terrestrial primary production  
1357 to the accuracy of meteorological reanalyses. *Journal of Geophysical Re-  
1358 search*, 111(G1), G01002. Retrieved from <http://doi.wiley.com/10.1029/2004JG000004> doi: 10.1029/2004JG000004  
1359  
1360 Zhu, X., Pei, Y., Zheng, Z., Dong, J., Zhang, Y., Wang, J., ... Xiao, X. (2018).  
1361 Underestimates of grassland gross primary production in MODIS standard  
1362 products. *Remote Sensing*, 10(11). doi: 10.3390/rs10111771